KALMAN FILTER BASED STATE AND PARAMETER ESTIMATOR APPLICATIONS IN DC/DC CONVERTER SYSTEMS

A THESIS SUBMITTED TO
THE GRADUATE SCHOOL OF NATURAL AND APPLIED SCIENCES
OF
MIDDLE EAST TECHNICAL UNIVERSITY

BY

MUHAMMED YUSUF CANDAN

IN PARTIAL FULFILLMENT OF THE REQUIREMENTS
FOR
THE DEGREE OF MASTER OF SCIENCE
IN
ELECTRICAL AND ELECTRONICS ENGINEERING

FEBRUARY 2021

Approval of the thesis:

KALMAN FILTER BASED STATE AND PARAMETER ESTIMATOR APPLICATIONS IN DC/DC CONVERTER SYSTEMS

submitted by **MUHAMMED YUSUF CANDAN** in partial fulfillment of the requirements for the degree of **Master of Science in Electrical and Electronics Engineering Department, Middle East Technical University** by,

Prof. Dr. Halil Kalıpçılar
Dean, Graduate School of **Natural and Applied Sciences** __________

Prof. Dr. İlkay Ulusoy
Head of Department, **Electrical and Electronics Engineering** __________

Assist. Prof. Dr. Mustafa Mert Ankaralı
Supervisor, **Electrical and Electronics Engineering, METU** __________

Examining Committee Members:

Assoc. Prof. Dr. Emre Özkan
Electrical and Electronics Engineering, METU __________

Assist. Prof. Dr. Mustafa Mert Ankaralı
Electrical and Electronics Engineering, METU __________

Assoc. Prof. Dr. Ozan Keysan
Electrical and Electronics Engineering, METU __________

Assist. Prof. Dr. Emine Bostancı
Electrical and Electronics Engineering, METU __________

Prof. Dr. Mehmet Timur Aydemir
Electrical and Electronics Engineering, Kadir Has University __________

Date: 10.02.2021

I hereby declare that all information in this document has been obtained and presented in accordance with academic rules and ethical conduct. I also declare that, as required by these rules and conduct, I have fully cited and referenced all material and results that are not original to this work.

Name, Surname: Muhammed Yusuf Candan

Signature :

ABSTRACT

KALMAN FILTER BASED STATE AND PARAMETER ESTIMATOR APPLICATIONS IN DC/DC CONVERTER SYSTEMS

Candan, Muhammed Yusuf
M.S., Department of Electrical and Electronics Engineering
Supervisor: Assist. Prof. Dr. Mustafa Mert Ankaralı

February 2021, 77 pages

In this thesis, we presented Kalman Filter based control methods for two different DC/DC converter systems. In the first application, we proposed an observer-based control method for sensorless output voltage regulation of a Full-Bridge converter. We introduced the modeling and design of the proposed observer-based control policy, and we demonstrated its performance and robustness through simulation experiments. Secondly, we proposed an hybrid Extended Kalman Filter based state, parameter (load resistance), and operation mode estimator for the Buck converter. Through extensive modeling and simulation studies, we showed that the algorithm can predict the operation mode effectively and estimate the states and unknown load resistance accurately. We believe that these studies can contribute the development of more robust, high-performance and sensorless voltage control policies for DC/DC converter topologies.

Keywords: Buck, Converter, DC/DC, Full-Bridge, Kalman Filter, Sensorless Control

ÖZ

DA/DA ÇEVİRİCİ SİSTEMLERİNDE KALMAN FİLTRE TABANLI DURUM VE PARAMETRE TAHMİNCİSİ UYGULAMALARI

Candan, Muhammed Yusuf
Yüksek Lisans, Elektrik ve Elektronik Mühendisliği Bölümü
Tez Yöneticisi: Dr. Öğr. Üyesi. Mustafa Mert Ankaralı

Şubat 2021 , 77 sayfa

Bu tezde, iki farklı DA/DA çevirici sistemi için Kalman Filtre tabanlı kontrol metotları sunduk. İlk uygulamada, Tam-Köprü çeviricinin çıkış geriliminin sensörsüz regülasyonu için gözlemci-tabanlı bir kontrol metodu önerdik. Sistemin modellemesini, sunulan gözlemci-tabanlı kontrol yönteminin tasarımını ve benzetim deneyleriyle performansını ve sağlamlığını tanıttık. İkinci olarak, Buck çevirici için hibrit Genişletilmiş Kalman Filtre tabanlı durum, parametre (yük direnci) ve operasyon modu tahmincisi sunduk. Kapsamlı modelleme ve benzetim çalışmaları aracılığıyla, geliştirilen algoritmanın operasyon modunu etkin bir şekilde öngördüğünü, durumları ve bilinmeyen yük direncini isabetli olarak tahmin edebildiğini gösterdik. Bu çalışmaların, DA/DA çevirici topolojileri için daha sağlam, yüksek performanslı ve sensörsüz gerilim kontrol metotlarının gelişmesine katkı sağlayacağına inanıyoruz.

Anahtar Kelimeler: Buck, Çevirici, DA/DA, Tam-Köprü, Kalman Filtre, Sensörsüz Kontrol

to my beloved wife Yasemin Özlem Nur...

ACKNOWLEDGMENTS

I would like to express my sincere appreciation and deep gratitude to my supervisor Assist. Prof. Dr. Mustafa Mert Ankaralı for his significant support, invaluable guidance and constant encouragement during my graduate work under his supervision.

For their valuable comments and criticism, I would also like to thank the examining committee members; Prof. Dr. M. Timur Aydemir, Assoc. Prof. Dr. Emre Özkan, Assoc. Prof. Dr. Ozan Keysan and Assist. Prof. Dr. Emine Bostancı.

I am grateful to Aselsan Inc. and my colleagues for their encouragement and support during my graduate studies.

I would like to thank my friends Furkan Karakaya, Osman Kaan Karagöz, Mustafa Murat Sezer, İbrahim Tayyip İşler, Hasan Burhan Beytur and Halil İbrahim Uğurlu for their valuable advice through my academic journey.

I would like to express my thanks to my loving mother Halime, to my dear father Orhan, to my dear brother Mustafa and to my loving grandparents, for their love, care and support.

I owe my loving thanks to my beloved wife Yasemin Özlem Nur because without her love, support and confidence in me, I would not have been able to run my business life and my graduate studies properly together. I shall always remember her respect and patience for my works.

All Praise is for Allah, by whose favor good works are accomplished.

TABLE OF CONTENTS

LIST OF TABLES

TABLES

LIST OF FIGURES

FIGURES

LIST OF ABBREVIATIONS

AC	Alternating Current
ADC	Anolog-to-Digital Converter
CCM	Continuous Conduction Mode
DC	Direct Current
DCM	Discontinuous Conduction Mode
DCR	Direct Current Resistance
DSP	Digital Signal Processor
EKF	Extended Kalman Filter
EMI	Electromagnetic Interference
ESR	Equivalent Series Resistance
KF	Kalman Filter
LPF	Low-Pass Filter
NRMSD	Normalized Root-Mean-Square Deviation
OIPSFB	Output Inductor-less Phase-Shifted Full-Bridge
PI	Proportional-Integral
PID	Proportional-Integral-Derivative
PSFB	Phase-Shifted Full-Bridge
PWM	Pulse Width Modulation
UKF	Unscented Kalman Filter
S&H	Sample and Hold
SMPS	Switch-Mode Power Supply

LIST OF VARIABLES

α	Mode band coefficient
ω_0	Resonant frequency of LC filter
ω_k	Process noise of the system at time k
ε	Current decay interval
C	Output filter capacitance
d	Effective duty cycle of primary voltage
f_c	1^{st} order low-pass filter cut-off frequency
f_s	Sampling frequency
f_{sw}	Switching frequency
f_k	System equation
g	Load conductance change
G_{load}	Nominal output load conductance
h_k	Measurement equation
i_f	Rectified-filtered-scaled primary current
$i_{f,est}$	Estimate of i_f
$i_{f,meas}$	Measurement of i_f
i_L	Inductor current
$i_{L,est}$	Estimate of i_L
i_O	Output load resistance current
$i_{O,meas}$	Measurement of i_O
$i_{O,samp}$	Sample of $i_{O,meas}$
i_{pri}	Transformer primary current
i_{sec}	Secondary side / output current

k	Sampling number
K_k	Kalman gain
L	Secondary side referred effective inductance
L_{pri}	Total primary inductance
m	Current transformer turns ratio
M	Primary current scaling factor
$mode$	Mode of a DC/DC converter system
$mode_{est}$	Estimate of $mode$
n	Transformer turns ratio
P_k	Co-variance of state estimation error
P_O	Rated output power
Q_k	Process noise co-variance matrix
r	Load resistance change
R	Output load resistance
R_{est}	Estimate of R
R_k	Measurement noise co-variance matrix
R_{load}	Nominal output load resistance
T_{sec}	Secondary side referred switching period for a Full-Bridge
T_{sw}	Switching period
u_k	Control input of a system
v_C	Capacitor voltage
$v_{C,est}$	Estimate of v_C
$v_{C,meas}$	Measurement of v_C
v_k	Measurement noise of a system at time k
v_m	Manipulated voltage for a Buck converter
v_{pwm}	Pulse-Width-Modulated voltage
V_D	Input voltage

V_O	Output voltage of a DC/DC converter
V_S	Secondary side referred input voltage
x_k	State vector of a system
y_k	Output of a system
Z_0	Characteristic impedance of LC filter

CHAPTER 1

INTRODUCTION

1.1 Motivation of the Thesis

Ned Mohan describes the task of power electronics as process and control the flow of electric energy by supplying voltages and currents in a form that is optimally suited for user loads [1]. In a broad sense, Figure 1.1 shows a general power electronic system block diagram which clearly depicts the explanation of its task.

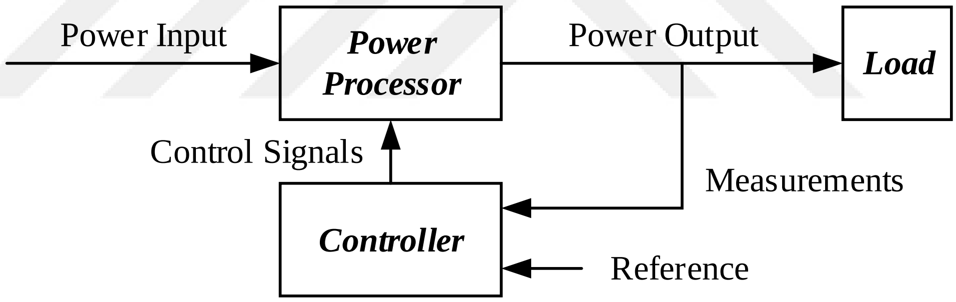

Figure 1.1: A general block diagram of a power electronic system [1]

The power processors in the above figure usually consist of more than one power conversion stage and we will refer to each power conversion stage as a converter. So, a converter is a building block of power electronic systems which utilize power semiconductor devices and possibly energy storage elements such as inductors and capacitors [1].

Considering the electrical form being Alternating Current (AC) or Direct Current (DC) on the input and output sides, we divide converters into the following categories:

- AC/DC (*also called as Rectifier*)
- DC/AC (*also called as Inverter*)
- DC/DC
- AC/AC

Within the scope of this thesis, we specifically deal with DC/DC converters. In a DC/DC converter (see Figure 1.2), the DC input voltage (typically unregulated) is converted to a DC output voltage with a larger or smaller magnitude and possibly with isolation of the input and output ground references [3].

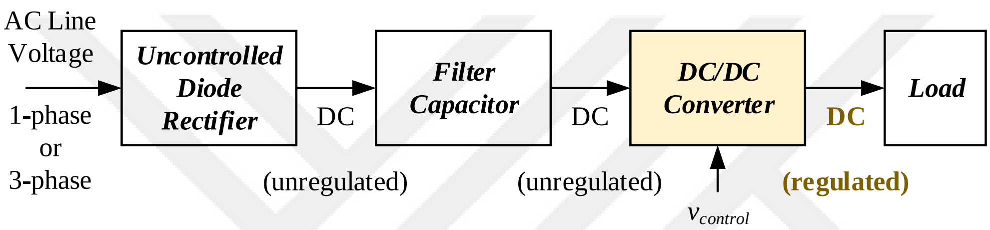

Figure 1.2: Block diagram of a power system with a DC/DC converter which converts and regulates an unregulated DC voltage

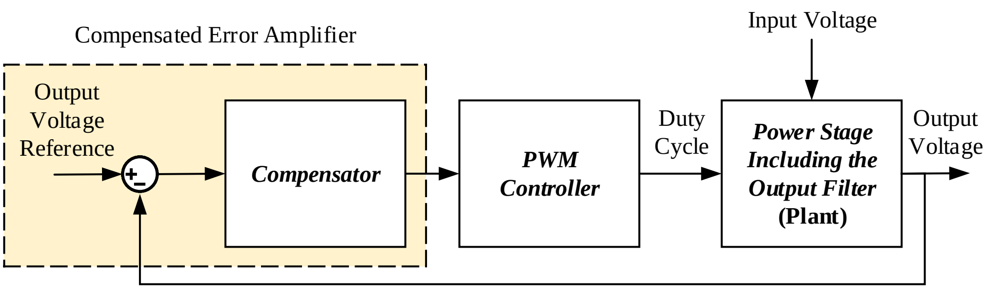

Figure 1.3: A general voltage feedback control system with a compensated error amplifier which regulates the output voltage of the power stage

The user load generally needs regulated output voltage meaning that it should be constant in case of possible input line voltage and load variations as well as disturbances. This regulation is accomplished by using a negative-feedback control system where the converter output voltage measurement is compared with its desired reference value and the error amplifier produces the proper control input [1] which is duty cycle of a switching regulator's Pulse Width Modulation (PWM) most of the time. Moreover, control input varies for different converter topologies such as phase-shift or switching frequency. Figure 1.3 depicts a general block diagram for a converter voltage feedback controller system.

Power electronic systems have analog and digital controller solutions. Until recently, due to low cost and ease of use, the control of converters were usually based on analog solutions [4]. Although the analog control technology is still pervasive in this field, some of the applications have very complex control and monitoring tasks which revive the need for digital control solutions. Digital control methods and digital controllers based on microprocessors, Digital Signal Processors (DSP's) or programmable logic devices have become very common in power electronics applications over the last two decades [5]. Figure 1.4 shows a possible digital control architecture with specialized blocks to meet the high-performance regulation requirements, as well as to solve monitoring and programming tasks through system interface [5].

Briefly, for the power electronic systems the advantages of digital controllers comparing with analog counterparts can be listed as follows [4]:

- Higher density
- Significantly reduced cost
- Help to improve system reliability and to eliminate drift and electromagnetic interference (EMI) problems
- Support of flexible software design (easy to update when the requirements change)
- Easier to test and debug

For the compensated error amplifier in Figure 1.3, the most common and straightforward choice to regulate the output voltage of the system is the Proportional-Integral-Derivative (PID) controller (see Figure 1.5). Although it can be developed in an

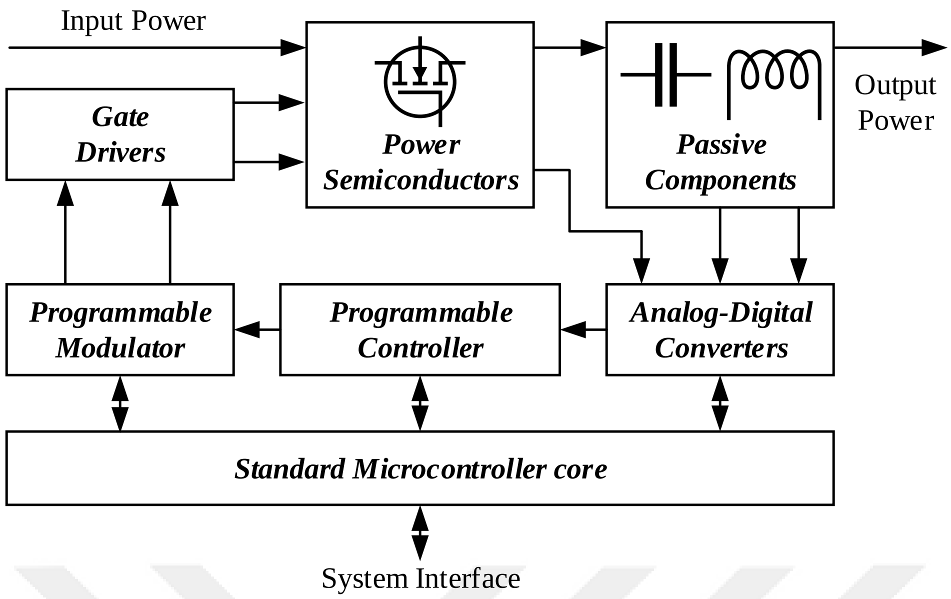

Figure 1.4: A digital Switch-Mode Power Supply controller architecture together with a converter power stage which consists of power semiconductor devices and passive filtering components

analog circuit hardware, tuning of the controller is much more easier in digital software environment. Utilization of the digital controllers simplifies not only the implementation of the PID controller but also other control methods to close the negative feedback loop. To design a proper controller to regulate the output voltage, we need the mathematical model of the converter system. Considering the control system performance criteria (rise time, settling time and over/under shoots) controller parameters are tuned according to the model. Typical controllers are designed based on small-signal models. Figure 1.6 shows the linearized feedback control system version of Figure 1.3. So, these models are valid around a particular operating point [6] which most of the time considered to be the nominal conditions of the converter. As an example, a converter may operate in half of the rated power, but in small-signal modeling, it is assumed that it operates in rated power.

However, the system does not have to be working at nominal conditions all the time. More importantly, changing the operating conditions of the system may cause converter model to change from one state to another. As an example, the Buck converter

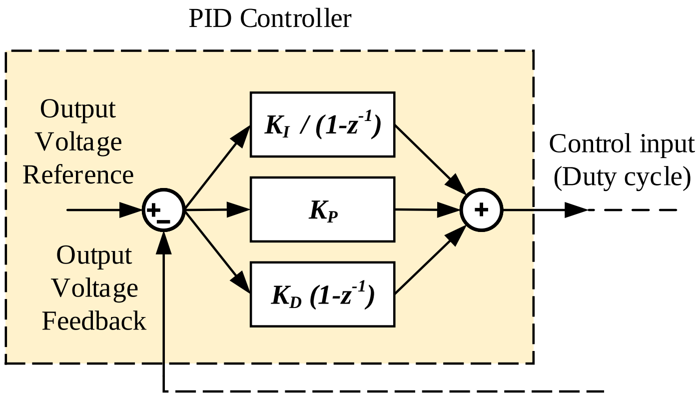

Figure 1.5: The conventional structure of the discrete-time Proportional-Integral-Derivative controller (in z-domain) where K_P is the coefficient of the term which is proportional to the current error value, K_I is the coefficient of the term accounting for past error values and K_D is the coefficient of the estimate term of the future trend of error

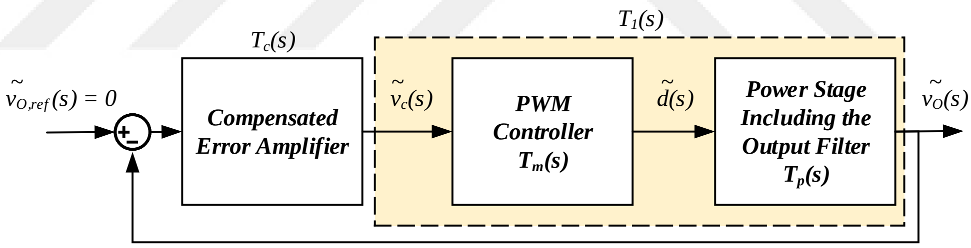

Figure 1.6: A general linearized voltage feedback control system with a compensated error amplifier transfer function $T_c(s)$ which regulates the output voltage of the power stage where $T_1(s)$ is plant system transfer function

(most popular non-isolated step-down DC/DC converter topology) shows a linear second-order characteristic in Continuous Conduction Mode (CCM) [7, 8], on the other hand, it exhibits nonlinear first-order system dynamics in Discontinuous Conduction Mode (DCM) [9]. Below figure shows the Buck converter circuit diagram and inductor current conduction modes.

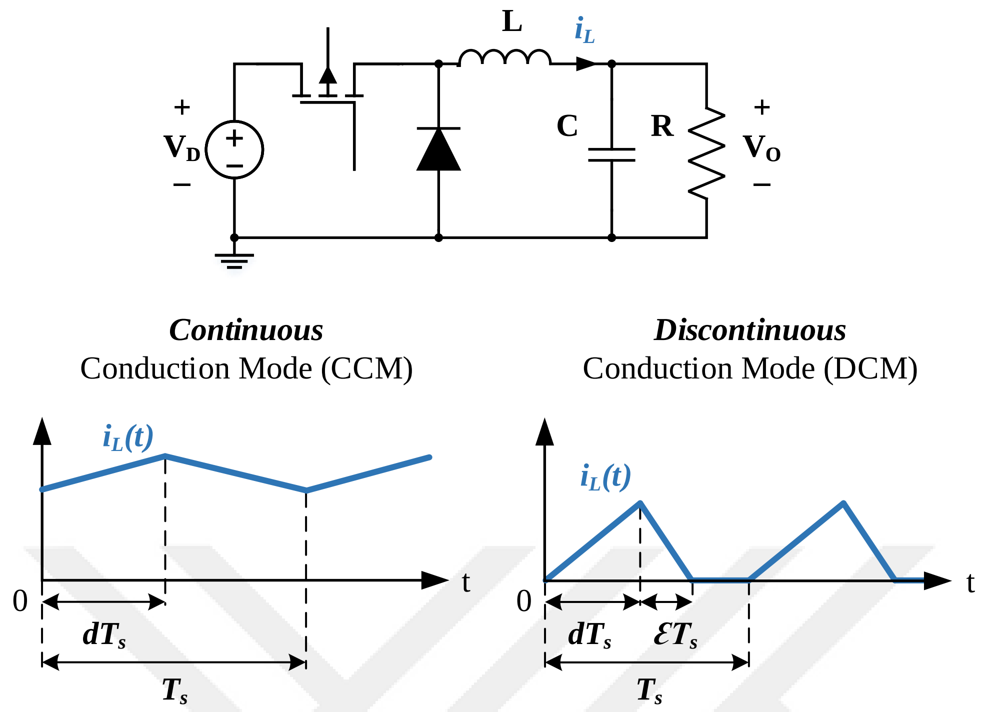

Figure 1.7: Circuit diagram and inductor current plots for Continuous Conduction Mode and Discontinuous Conduction Mode of Buck converter

If deviations from assumed particular operating point destabilize the system, adaptive control methods have to be considered. For the given example, operating mode information is important for an adaptive controller. However, the mode of operation and other parameters causing significant model deviations may not be directly measured unlike voltages and currents.

An observer may be incorporated in the control of a system in cases where system state vector is not available for measurement [10, 11]. However, aforementioned parameters are not directly defined as system's states. So, an improved observer algorithm should be utilized to estimate these parameters.

In 1960, Rudolf E. Kálmán published his now-popular paper, "A New Approach to Linear Filtering and Prediction Problems" [2] which significantly contributed to the field of linear filtering.

Rudolf E. Kálmán proposed a powerful estimation algorithm. Although the algorithm, commonly known as Kalman Filter (see Figure 1.8), was utilized in aerospace applications at the first place, the relative simplicity and versatility of its formulation resulted in the algorithm to rapidly adapt for utilization in many other fields. Leonard McGee and Stanley Schmidt state that the Kalman Filter in its various forms is clearly established as a fundamental tool for analyzing and solving a broad class of estimation problems [12].

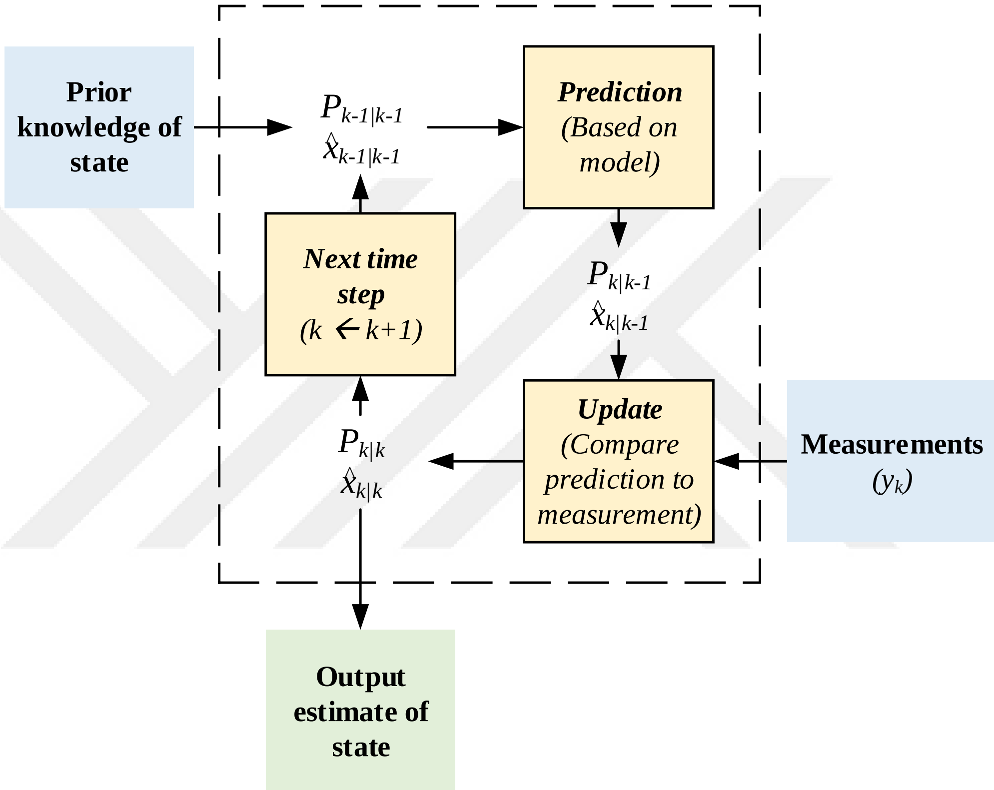

Figure 1.8: The diagram explains the basic steps of Kalman Filter algorithm: prediction and update. Here, $\hat{x}$ is the state estimate, P is the covariance matrix; $k-1|k-1$ denotes *a priori* knowledge, $k|k$ sub-script denotes *a posteriori* estimate at time k given observations up to and including at time k, $k|k-1$ sub-script denotes estimate at time step k before the $k-th$ measurement y_k has been taken into account [2].

Kalman Filter is an estimation algorithm which uses a series of noisy and most probably inaccurate data measured over time to estimate states and unknown variables with more accuracy [13]. The algorithm operates by propagating the mean and covariance of the state through time [2, 14]. And one of the remarkable aspect of this algorithm is that it is optimal in several different senses [14]. Figure 1.8 illustrates the diagram of the basic steps of Kalman Filtering. The diagram also shows how the algorithm keeps track of not only the mean of the state, but also the estimated variance. $\hat{x}_{k|k-1}$ denotes the estimate of the system's state at time step k before the $k-th$ measurement y_k has been utilized and $P_{k|k-1}$ is the corresponding uncertainty [2].

State estimation theory can be utilized not only to estimate the states but also to estimate the unknown parameters of a system [14] and this may have first been suggested in [15]. The unknown system parameters can be considered as additional states. Using noise-contaminated data, both system parameters as well as the system states can be estimated [15].

As discussed before, for a wide load range application of a DC/DC converter where the system model changes due to significant change in the load current, it is useful to know in which mode system operates. The controller can be designed in a way that it adapts itself according to mode. An appropriate form of Kalman Filter can be utilized to estimate the required system parameter. As an example, Figure 1.9 shows a load resistance estimation result of Buck converter study in this thesis. Actually, Kalman Filter is a type of state observer but it is designed for stochastic systems instead of deterministic systems. So, algorithm needs system's process and measurement noise co-variances to proceed. Although it is not considered most of the time, power electronic systems have process and measurement noises in their nature. In addition to well defined model of the converter, its noise characteristics should be determined properly. Then, we can utilize it to estimate the parameters in our interest.

Most of the time the unknown non-state parameters have nonlinear relationships with actual states of the model. But standard Kalman Filter algorithm can only be applied to linear systems. Because of similar reasons, the scientific breakthroughs and reformulations were necessary to transform Kalman's work into a useful tool for specific applications [12].

Different types of Kalman Filter algorithm have been developed until today. They are mainly Kalman Filter (KF), Extended Kalman Filter (EKF) and Unscented Kalman Filter (UKF). And specifically, the Extended Kalman Filter algorithm is an optimal

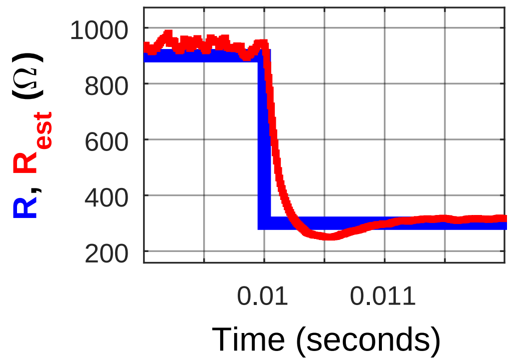

Figure 1.9: Simulation results showing Buck converter load resistance estimation (R_{est}) with respect to actual value (R) for a transition instant

recursive estimation algorithm for nonlinear systems [16].

Selection of the algorithm depends on requirements and computational limits. In this thesis, there are mainly two separate studies where we make use of different types of Kalman Filter. We explain problem definitions and contributions of these studies in the following two subsections.

1.2 Problem Definition and Contribution of the Full-Bridge Converter Study

In the first study of this thesis, we utilize Kalman Filter to estimate output voltage of a Full-Bridge (an isolated DC/DC) converter. Unlike conventional feedback control, we propose to regulate the output voltage without directly measuring it. Instead, we estimate it by measuring filtered primary current state. Figure 1.10 shows the basic general diagram of this study.

There are two main motivations behind this study.

First of all, for some of the isolated converter applications, the isolation level (mostly described in terms of isolation capacitance) has critical importance. Since the references of two sides (namely primary and secondary sides of the converter) are isolated, the output voltage feedback is provided by opto-isolation most of the time. There are examples of non-regulated highly isolated DC/DC converters, which means that the requirement of isolation can become so critical that the regulation may be omitted.

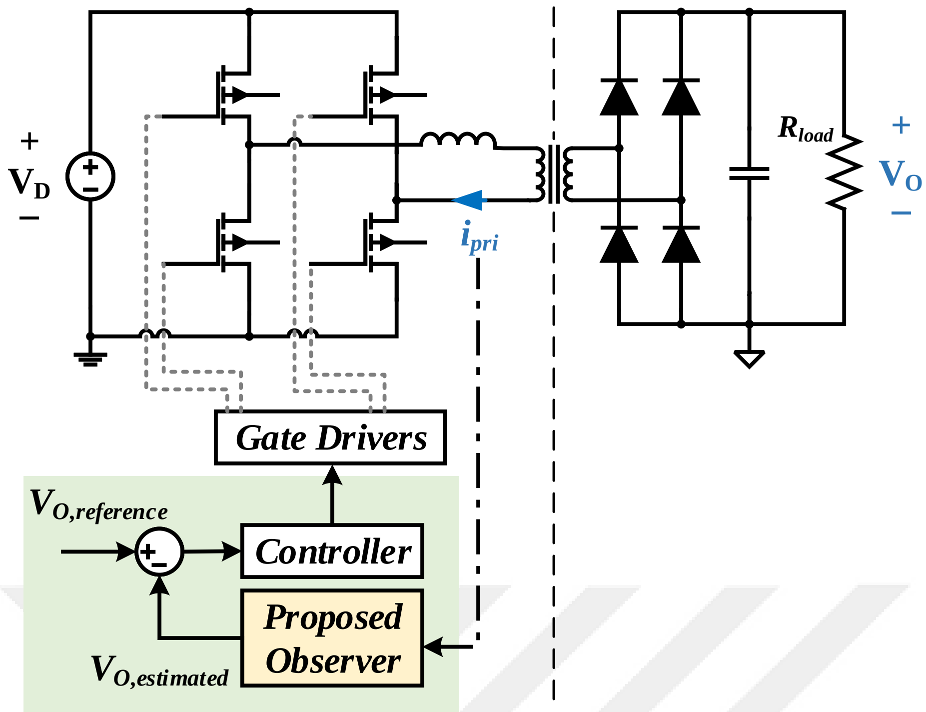

Figure 1.10: The basic diagram of proposed observer based output voltage control of a Full-Bridge converter

Even for redundancy or at least increasing the regulation quality of the converter, we propose a solution to estimate the output voltage which can be fed back to control system.

This method can also be applied to wireless power converters [17] which are also isolated converters. Although their model are different from the model of the topology that we investigated in this study, the method that we propose can be modified and may be applied to these topologies. Because in some of their applications the feedback of the output voltage is provided through Radio Frequency Identification (RFID) which has some limitations like frequency range limitation for underwater applications. Since electromagnetic waves can not travel through electrical conductors, in most of the time, radio waves are not suitable for underwater communication [18].So, even for the redundancy, our proposed method can be applied to those systems.

One of the contributions of this study is that the proposed method can estimate the output voltage of a Full-Bridge converter in varying load conditions, which reflects the practicality of our proposition.

1.3 Problem Definition and Contribution of the Buck Converter Study

In the second study, we utilize Kalman Filter to estimate the load resistance and operating mode of a Buck converter. We specifically investigate wide load range applications where operating point significantly diverges from supposed conditions, which changes system model. Figure 1.11 shows the basic idea of this study.

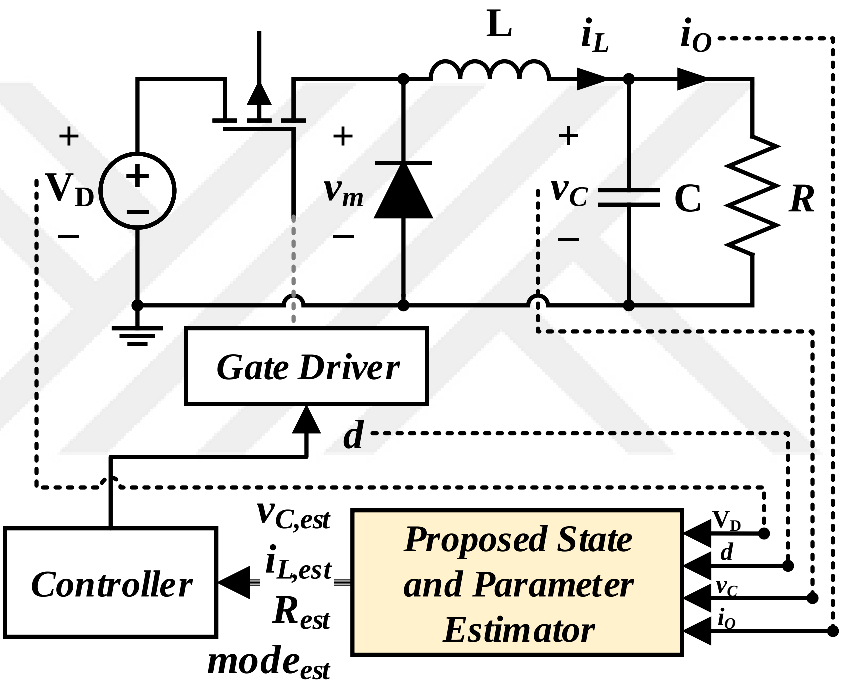

Figure 1.11: The basic diagram of utilization of proposed estimation method

There is one main motivation behind this study.

The vast majority of Buck converter modeling and control studies rely on the assumption that load resistance operates near a nominal value. Accordingly, controller and estimator designs in literature are mainly centered around the assumed nominal load resistance [19]. We propose Kalman Filter based state, parameter (load resistance), and operation mode estimator for Buck converter topology. Since, the proposed estimation algorithm can accurately work in both CCM and DCM operations, it can be utilized in adaptive controllers designed for wide load range applications.

One of the contributions of this study is that through extensive modeling and simulation studies, we show that the proposed algorithm can predict the operation mode effectively and estimate the states and unknown load resistance accurately in case of explicit process and measurement noise integrated environment.

1.4 The Outline of the Thesis

The organization of this thesis is as follows. Chapter 2 presents “Linearized Kalman Filter observer based control for a Full-Bridge DC/DC converter without output voltage measurement“ study. Then, Chapter 3 presents “Extended Kalman Filter based state and parameter estimation method for a Buck converter operating in a wide load range application“ study. In each of these two chapters, the discrete-time modeling of the aforementioned converter system and design of the estimator/observer based control policy are explained in detail. On the exemplary plant converter systems, the performance and robustness of the proposed algorithms are discussed upon related simulation studies. The Chapter 4 summarizes research results related to this thesis.

CHAPTER 2

LINEARIZED KALMAN OBSERVER BASED CONTROL FOR A FULL-BRIDGE DC/DC CONVERTER WITHOUT OUTPUT VOLTAGE MEASUREMENT

2.1 Introduction

The Phase-Shifted Full-Bridge (PSFB) DC/DC converter is one of the most preferable isolated converters in power electronics applications. Several studies proposed that a PSFB converter reduces stresses on components and switching losses compared to a hard-switching PWM Full-Bridge converter [20–22].

Particularly in high output voltage applications, PSFB converter has reverse recovery losses in the secondary rectifier diodes and high voltage ringing caused by the resonance between the diode parasitic capacitance and transformer leakage inductance [23–28]. However, in Output Inductorless Phase-Shifted Full-Bridge converter (OIPSFB) (see Figure 2.1) voltage stresses of the rectifier diodes can be clamped to the output voltage, which eliminates the need for dissipative RC snubber [24–26]. In this study, we focus on the OIPSFB converter topology, and develop a dynamic observer based control algorithm without measuring the output voltage.

Until recently, researchers proposed different control methods to regulate the output voltage in isolated DC/DC converters. One of the challenges for the control design is that the power devices of the converters have very complicated time-varying switching behavior. Therefore, the converter dynamic model development is a challenge. Secondly, DC/DC converters typically have a wide range of operating conditions, which further complicates the controller design process [29].

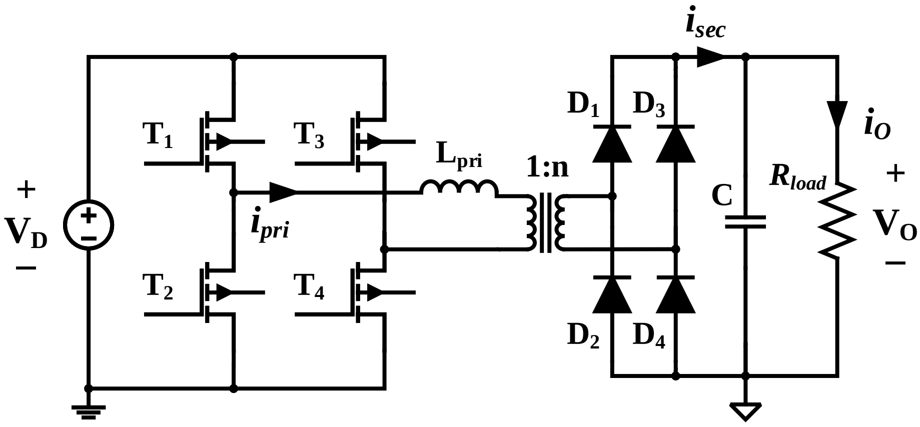

Figure 2.1: Circuit diagram of the Output Inductorless Phase-Shifted Full-Bridge DC/DC converter where L_{pri} represents the total primary inductance including the leakage of the transformer

Several studies [29–33] have proposed observer-based controllers for DC/DC converters to obtain a better dynamic performance in a wide range or to eliminate the need for current measurement. Ibrahim et al. [30] present a state observer-based feedback controller for a PSFB DC/DC converter to increase the dynamic performance of the closed-loop system. However, unlike our approach in this study, they still measure the output voltage for the state estimation & observation process. On the other hand, Xie et al. [29] investigate both Linear Model Predictive Control (LMPC) and Nonlinear Model Predictive Control (NMPC) schemes for the Full-Bridge DC/DC converter where they only measure the output voltage to satisfy regulation and peak current protection. Lu et al. propose an Enhanced State Observer (ESO) based DC-link voltage control strategy for a three-phase AC/DC converter in [31] and a Reduced Order Enhanced State Observer (RESO) based voltage control strategy for the voltage loop of the DC/DC Buck converter in [32]. Their common goal in both studies is to provide a high disturbance rejection ability and robustness against parameter variations without current measurement. There exist different approaches that also eliminate the requirement of the current measurement in DC/DC converters. For example, Beccuti et al. [34] propose an explicit Model Predictive Control (MPC) scheme for DC/DC power supplies, whereas Pandey et al. [33] adopt a State and Disturbance Observer (SDO) based algorithm for the control of DC/DC Boost converters.

One should note the fact that an almost standard approach in these studies is that they observe the current using the voltage measurement. However, in this study, we propose an observer-based controller without voltage measurement to remedy a different issue. One of the properties of the isolated converters is the isolation capacitance between the primary and secondary sides of the circuit. This capacitance is formed mainly from coupling capacitance in the converter transformer as well as from feedback optocoupler [35]. As we discussed above, for the regulation, the output voltage is measured, and the vast majority of these applications make use of an optocoupler isolation circuitry. In this context, our method provides voltage regulation without direct voltage measurement taking into account the need for low input-output isolation capacitance and regulated output voltage in case of input voltage and load resistance changes.

We approach the problem as closing the control loop with voltage estimation by Linearized Kalman Filter using manipulated primary current measurement. Although we introduce the method in an OIPSFB converter that nominally operates in Discontinuos Conduction Mode (DCM), we show that it can also work in Continuous Conduction Mode (CCM) of operation. We presented the modeling of the converter and design of the proposed observer-based control policy, and we demonstrated its performance in MATLAB Simulink environment.

2.2 Modeling of the Converter

Throughout the modeling, for the circuit in Figure 2.1:

- Assume that T_1, T_2, T_3, T_4, D_1, D_2, D_3, D_4 and converter transformer are ideal components.
- Ignore the Equivalent Series Resistance (ESR) of C and the DC Resistance (DCR) of L_{pri}.
- Assume that the resonant frequency of LC filter is low compared with the sampling frequency T_s ($\omega_0 T_s \ll 1$).
- Assume resistive loads.

In this study, we first develop the discrete-time dynamic model of the OIPSFB converter by referring the primary circuit to the secondary side. We refer input voltage V_D as V_S, total primary inductance L_{pri} as L and switching period T_{sw} as T_{sec} to the secondary side. Following set of equations describe the relationships between these parameters,

$$V_S = nV_D \tag{2.1}$$

$$L = n^2 L_{pri} \tag{2.2}$$

$$T_{sec} = T_{sw}/2 \tag{2.3}$$

Figure 2.2 illustrates the secondary side referred equivalent circuit diagram. Since we propose a method to provide output voltage regulation in case of any resistive load change, we design an observer being able to estimate the load changes, which we model as an additional series resistance (r) connected to the nominal load resistance (R_{load}). This approach simplifies obtaining a linearized circuit model around the nominal conditions. Also, for the model derivation, it is convenient to use nominal load conductance (G_{load}) and change in the load conductance (g) instead of resistance equivalencies.

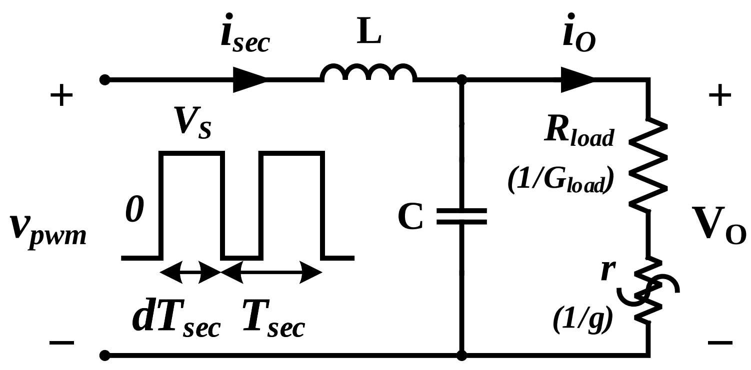

Figure 2.2: Secondary side referred OIPSFB converter circuit diagram where R_{load} represents the nominal load resistance and r is the change in the load resistance

In the model expressions, we use characteristic impedance and resonant frequency parameters of the effective LC filter given as

$$Z_0 = \sqrt{L/C} \tag{2.4}$$

$$\omega_0 = 1/\sqrt{LC} \tag{2.5}$$

Lim et al. [36] show that a regular sampling of the inductor current is not useful. The sampled current does not correspond to the short-time average value since the current shape is not symmetrical with respect to PWM carrier signal [37]. In this study, we measure the primary current i_{pri} through the current transformer, rectifier, and a 1^{st} order low-pass filter. The actual scaling of this value results in the mean current in the secondary side. So, regardless of the current being continuous or discontinuous, we have the information of the mean current of the effective inductor L.

As a next step, we derive the discrete-time dynamic model of the converter system. Broeck et al. [37] develop separate CCM and DCM models for a Buck converter where the duty cycle command for DCM accurately tracks both CCM and DCM regions. For DCM operation, they obtain a nonlinear first-order dynamics for the output voltage. We use a similar modeling approach; however, in our model, we have a new state variable of the average inductor current. The addition of the average inductor current as a state variable provides continuity in current information, which is the only measurement that we can utilize to observe the output voltage in our approach. Figure 2.3 depicts the sampling instants during discretizing the dynamics.

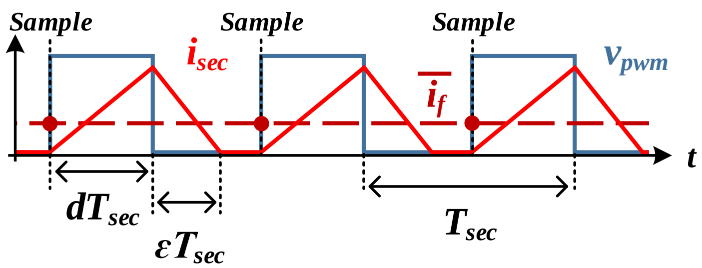

Figure 2.3: PWM voltage (v_{pwm}), secondary side current (i_{sec}) and sampling of rectified-filtered-scaled primary current (i_f) waveforms for DCM operation

Assuming $\omega_0 T_s \ll 1$ we have the following continuous time differential equations:

$$L\frac{di_{sec}(t)}{dt} = v_L(t) \tag{2.6}$$

$$C\frac{dv_O(t)}{dt} = i_C(t) \tag{2.7}$$

and solving these equations for effective inductor ($L = (\frac{\omega_0}{Z_0})^{-1}$) and output capacitor ($C = (Z_0\omega_0)^{-1}$) we obtain

$$\overline{v}_{pwm}(t) = d(kT_{sec})V_S \tag{2.8}$$

$$v_O(t) \approx v_O(0) + (i_{sec}(0) - i_O(0))Z_0\omega_0 t \tag{2.9}$$

$$i_{sec}(t) \approx i_{sec}(0) + (\overline{v}_{pwm}(0) - v_O(0))\frac{\omega_0}{Z_0}t \tag{2.10}$$

where $\overline{v}_{pwm}(t)$ is manipulated input voltage that is equal to the average voltage across input terminals of secondary side referred circuit within one switching cycle T_{sec}. Table 2.1 shows the characteristic instances of the current and voltage signals during one PWM period in DCM operation.

Table 2.1: Full-Bridge Converter Effective Inductor Current and Capacitor Voltage at the Characteristic Instances During One Pulse Width Modulation Period in Discontinuous Conduction Mode

$\mathbf{t_X}$	$\mathbf{v_O(kT_{sec} + t_X) =}$	$\mathbf{i_{sec}(kT_{sec} + t_X) =}$
$t_X = dT_{sec}$	$v_O(kT_{sec})-$ $i_O(kT_{sec})Z_0\omega_0 dT_{sec}$	$(V_S - v_O(kT_{sec}))\frac{dT_{sec}\omega_0}{Z_0}$
$t_X = (d+\varepsilon)T_{sec}$	$v_O(kT_{sec})(1-(\omega_0T_{sec})^2 d\varepsilon)-$ $Z_0\omega_0T_{sec}(\varepsilon+d)i_O(kT_{sec})+$ $(\omega_0T_{sec})^2(d\varepsilon)V_S$	0
$t_X = T_{sec}$	$v_O(kT_{sec})(1-(\omega_0T_{sec})^2 d\varepsilon)-$ $Z_0\omega_0T_{sec}i_O(kT_{sec})+$ $(\omega_0T_{sec})^2(d\varepsilon)V_S$	0

We use these approximated equations to determine the dynamics of the converter in DCM operation over one carrier interval. We trigger the calculation point at the instant when we switch on the Full-Bridge. During the active voltage pulse (dT_{sec} duration), the current i_{sec} increases up to the following peak value.

$$i_{sec}(kT_{sec} + dT_{sec}) = (V_S - v_O(kT_{sec}))\frac{dT_{sec}\omega_0}{Z_0} \tag{2.11}$$

After dT_{sec} time span, inductor current decays to zero. We need the current decay time (ε) given in (2.12) to calculate the output voltage at the end of the PWM interval (2.13).

$$\varepsilon(kT_{sec}) = \frac{(V_S - v_O(kT_{sec}))d(kT_{sec})}{v_O(kT_{sec}) - Z_0\omega_0 T_{sec} d(kT_{sec}) i_O(kT_{sec})} \tag{2.12}$$

$$\begin{aligned} v_O((k+1)T_{sec}) = v_O(kT_{sec}) - Z_0\omega_0 T_{sec} i_O(kT_{sec}) + \dots \\ \dots + \frac{d(kT_{sec})^2(\omega_0 T_{sec})^2(V_S - v_O(kT_{sec}))^2}{v_O(kT_{sec}) - Z_0\omega_0 T_{sec} i_O(kT_{sec}) d(kT_{sec})} \end{aligned} \tag{2.13}$$

As we stated before we have the average inductor current (i_f) state as well as output voltage (v_O) and load conductance change (g). System state vector becomes as

$$x[k] = \begin{bmatrix} i_f[k] & v_O[k] & g[k] \end{bmatrix}^T \tag{2.14}$$

For resistive load applications, the average inductor current is equal to the load current. So, instead of load current (i_O) in equation (2.13) we write the following,

$$i_O(kT_{sec}) = v_O(kT_{sec})(G_{load} + g(kT_{sec})) \tag{2.15}$$

Arranging the expressions we end up with the augmented model in equation (2.17). Linearizing it around the nominal conditions ($V_O, V_S, G_{load}, d_{nom}$) as in (2.16) we obtain the linearized discrete-time dynamic model in matrix form of (2.18).

$$F_k = \left.\frac{\partial f_k}{\partial x}\right|_{V_O, V_S, G_{load}, d_{nom}} \tag{2.16}$$

$$f_k = x[k+1] = \begin{bmatrix} i_f[k+1] \\ v_O[k+1] \\ g[k+1] \end{bmatrix} = \cdots$$
$$\cdots \begin{bmatrix} v_O[k](G_{load} + g[k]) \\ \frac{d[k]^2(\omega_0 T_{sec})^2(V_S[k]-v_O[k])^2}{v_O[k]-v_O[k](Z_0\omega_0 T_{sec})d[k](G_{load}+g[k])} - v_O[k](Z_0\omega_0 T_{sec})(G_{load} + g[k]) + v_O[k] \\ g[k] \end{bmatrix} \tag{2.17}$$

$$F_k = \begin{bmatrix} F_{k_{11}} & F_{k_{12}} & F_{k_{13}} \\ F_{k_{21}} & F_{k_{22}} & F_{k_{23}} \\ F_{k_{31}} & F_{k_{32}} & F_{k_{33}} \end{bmatrix} \tag{2.18}$$

$$F_{k_{11}} = F_{k_{21}} = F_{k_{31}} = F_{k_{32}} = 0 \tag{2.19}$$

$$F_{k_{12}} = G_{load} \tag{2.20}$$

$$F_{k_{13}} = V_O \tag{2.21}$$

$$F_{k_{22}} = 1 - (Z_0\omega_0 T_{sec})G_{load} + \frac{d_{nom}^2(\omega_0 T_{sec})^2}{1-(Z_0\omega_0 T_{sec} d_{nom})G_{load}} \cdot \frac{V_O^2 - V_S^2}{V_O^2} \tag{2.22}$$

$$F_{k_{23}} = \frac{d_{nom}^2(\omega_0 T_{sec})^2(V_S - V_O)^2 Z_0\omega_0 T_{sec} d_{nom} V_O}{(V_O - Z_0\omega_0 T_{sec} d_{nom} V_O G_{load})^2} - Z_0\omega_0 T_{sec} V_O \tag{2.23}$$

$$F_{k_{33}} = 1 \tag{2.24}$$

2.3 Linearized Kalman Filter Based Observer Design

In this study, we use the discrete-time linearized Kalman Filter to observe the output voltage (v_O) and change in the load conductance (g) from the average inductor current measurement (i_f). Figure 2.4 illustrates the generalized block diagram of the proposed method.

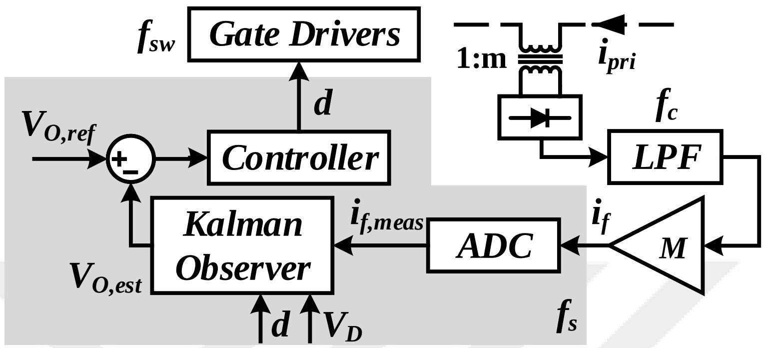

Figure 2.4: Diagram shows the proposed observer-based sensorless voltage controller for a Full-Bridge DC/DC converter. Primary current is scaled through current transformer, then it is rectified and filtered. Utilizing a discrete-time Linearized Kalman Observer, the output voltage is estimated and fed-back to control system.

Figure 2.5 details the Linearized Kalman Filter based observer algorithm for a generic nonlinear discrete-time state-space model, where hat symbol $(\hat{.})$ denotes estimate, plus superscript $(.^{+})$ denotes *a posteriori* (after the measurement correction update) and minus superscript $(.^{-})$ denotes *a priori* (before the measurement correction update) along with state (x_k) and error co-variance (P_k) at sub-scripted time k [14].

We have obtained a nonlinear discrete-time model for the system in Sec. 2.2. When we adopt the proposed algorithm to the derived model, the linearized Kalman estimator filters out the noise of the measured current (i_f), observes the output voltage (v_O) and estimates the change in the load conductance (g) in the presence of process and measurement noises. We calculate the total output load resistance estimate (R_{est}) as in (2.25). Here, notice that g_{est} is change in load conductance.

$$R_{est} = \frac{1}{G_{load} + g_{est}} \tag{2.25}$$

Dynamic System Equations

$$x_k = f_{k-1}(x_{k-1}, u_{k-1}, \omega_{k-1})$$
$$y_k = h_k(x_k, v_k)$$
$$\omega_k \sim (0, Q_k)$$
$$v_k \sim (0, R_k)$$

Initialization

$\hat{x}_o^+$ *and* P_0^+

Compute $F_{k-1} = \frac{\partial f_{k-1}}{\partial x}|_0$ and $H_k = \frac{\partial h_k}{\partial x}|_0$

For $k = 1,2,\cdots$

Prediction

1. State projection (*a priori* state estimate)

$$\hat{x}_k^- = f_{k-1}(\hat{x}_{k-1}^+, u_{k-1}, 0)$$

2. Error covariance projection

$$P_k^- = F_{k-1}P_{k-1}^+F_{k-1}^T + Q_{k-1}$$

Correction

1. Kalman gain computation

$$K_k = P_k^- H_k^T \left(H_k P_k^- H_k^T + R_k\right)^{-1}$$

2. Estimation update with measurement y_k (*a posteriori* state estimate)

$$\hat{x}_k^+ = \hat{x}_k^- + K_k[y_k - h_k(\hat{x}_k^-, 0)]$$

3. Error covariance update

$$P_k^+ = (I - K_k H_k)P_k^-$$

Figure 2.5: Discrete-time Linearized Kalman Filter algorithm

2.4 Controller Design

We prefer using PID controller in this application and we design the controller based on the discrete time model. We tune the coefficients by determining crossover frequency and phase margin requirements, then observing overshoot and settling time of the responses. Comparing the results we select the best controller in between different options.

Figure 2.6 shows open loop bode diagram (from duty cycle to output voltage) of the discrete-time converter system for nominal load condition ($R = 90\Omega$).

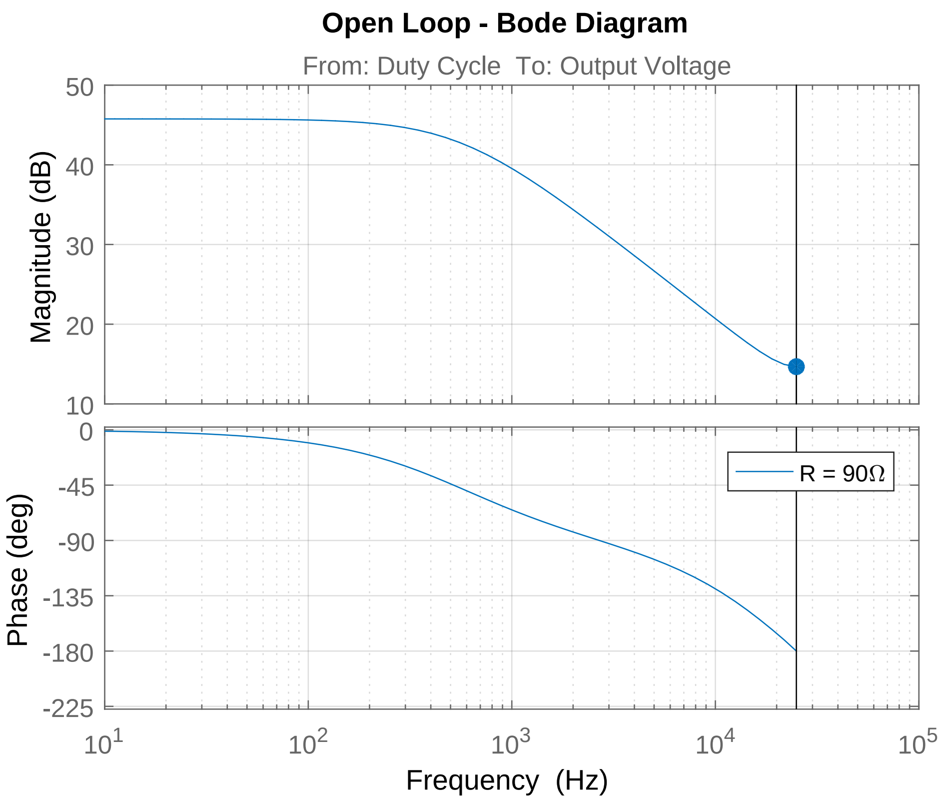

Figure 2.6: Open loop bode diagram of the discrete-time Output Inductor-less Phase-Shifted Full-Bridge converter system for nominal load condition. Here, gain margin is $-14.7dB$ at frequency of $25kHz$ and the system is not stable.

Investigating the open loop bode plot, we decide to use a PI controller. For different crossover frequencies, we tune PI coefficients for better disturbance rejections. Figure 2.7 shows step responses for different PI controllers and Table 2.2 gives corresponding coefficients and details of these responses.

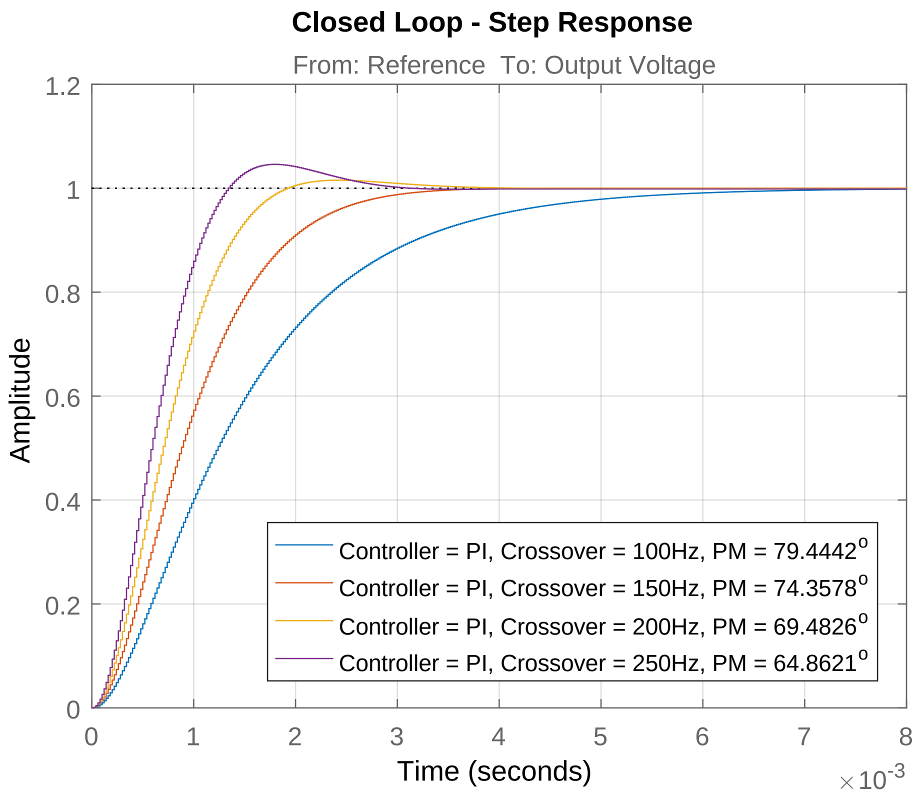

Figure 2.7: Step responses of the discrete-time Full-Bridge converter system for different PI controllers

Table 2.2: Controller Options for Full-Bridge Converter System

K_P	K_I	T_s (sec)	Crossover Frequency (Hz)	Phase Margin $(^o)$	Overshoot (%)	Settling Time $(msec)$
3.29×10^{-5}	3.29	2×10^{-5}	100	79.4442	0	5.06
5.03×10^{-5}	5.03	2×10^{-5}	150	74.3578	0.00207	2.77
6.87×10^{-5}	6.87	2×10^{-5}	200	69.4826	1.54	1.73
8.86×10^{-5}	8.86	2×10^{-5}	250	64.8621	4.59	2.43

We select the 3^{rd} controller in Table 2.2 considering both overshoot and settling time performances. Figure 2.9 shows controlled system (see definition in Figure 2.8) bode diagram for the following PI coefficients:

$$
\begin{aligned}
K_P &= 6.87 \times 10^{-5}\,, \\
K_I &= 6.87\,, \\
T_s &= 2 \times 10^{-5}\,.
\end{aligned}
\tag{2.26}
$$

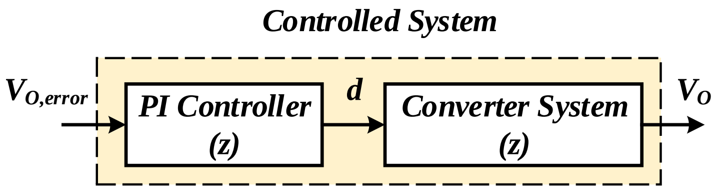

Figure 2.8: "Controlled System/Plant" definition

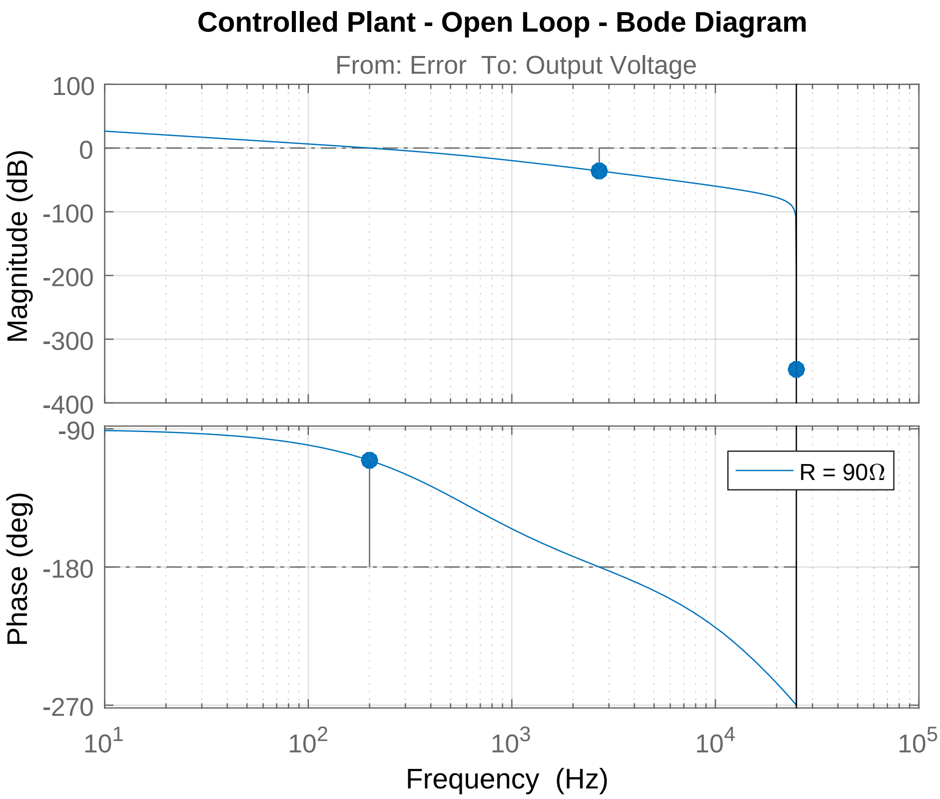

Figure 2.9: Bode diagram of the controlled discrete-time Output Inductor-less Phase-Shifted Full-Bridge converter system with selected PI controller. Here, phase margin is $69.5dB$ at frequency of $200Hz$ and the system is stable.

2.5 Simulation Results

Figure 2.10 illustrates the simulation environment and how we integrate the process and measurement noises to current and voltage states inside the circuit simulation.

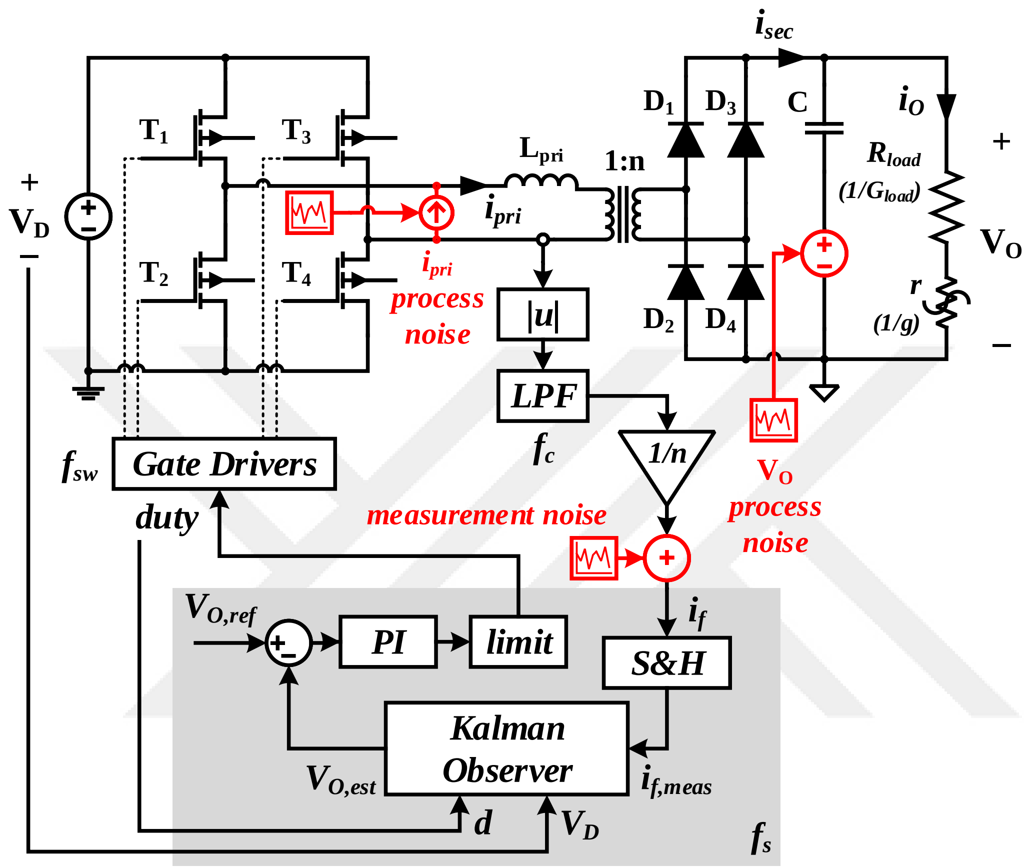

Figure 2.10: Simulation environment diagram showing process and measurement noise addition to the states (note that we take the primary current scaling factor (M) as $1/n$ and we use Sample and Hold (S&H) block instead of Analog-to-Digital Converter (ADC))

For the simulation studies, we assume that we know the process and measurement noise co-variances (Q_k and R_k matrices) apriori in the algorithm. Even though in the simulation scenario, the load conductance change parameter (g) trajectories are deterministic, the Kalman Filter algorithm still needs a small artificial noise term allowing the Kalman Filter to change its estimate of the parameter [14]. We accept all the required assumptions given at the beginning of the modeling part and simulate the circuit and observer algorithm in MATLAB Simulink environment. Instead of an average model, we simulate the circuit using *Simscape/Power Systems/Specialized Technology* library in Simulink, which brings unmodeled effects such as transistor resistance, diode resistance, and forward voltage. Although this implies that the simulated circuit is not ideal as stated in the modeling part, promising simulation results show that we can use this method in the presence of unmodeled and potentially nonlinear dynamic uncertainties. We provide the adopted converter circuit parameters in Table 2.3 and observer system parameters in Table 2.4.

Table 2.3: Circuit Parameters for the Full-Bridge Converter Study

Input voltage	V_D = 28 V
Output voltage	V_O = 150 V
Rated output power	P_O = 250 W
Total primary inductance	L_{pri} = 1.75 μH
Output filter capacitance	C = 10 μF
Switching frequency	f_{sw} = 50 kHz
Transformer turns ratio	n = 10 turns

Table 2.4: Observer System Parameters, Process and Measurement Noise Co-variances for the Full-Bridge Converter Study

LPF cut-off frequency	f_c = 1 kHz
Sampling frequency	f_s = 50 kHz
Current transformer turns ratio	m = 1 turn
Primary current scaling factor	M = 0.1
Process noise co-variance	$Q_k = \begin{pmatrix} 10^{-4} & 0 & 0 \\ 0 & 10^{-3} & 0 \\ 0 & 0 & 10^{-9} \end{pmatrix}$
Measurement noise co-variance	$R_k = \begin{pmatrix} 5 \times 10^{-3} \end{pmatrix}$

Taking into account the practical concerns we sample the current at each PWM period interval. In fact we model the circuit by referring to the secondary side where the frequency doubles, which does not bring inaccuracy as results illustrate. Figure 2.11

presents the sampling of the filtered current i_f. Trigger of the Sample and Hold (S&H) block is the rising edge of T_1 gate signal. Estimated current is the average of the secondary side current (i_{sec}).

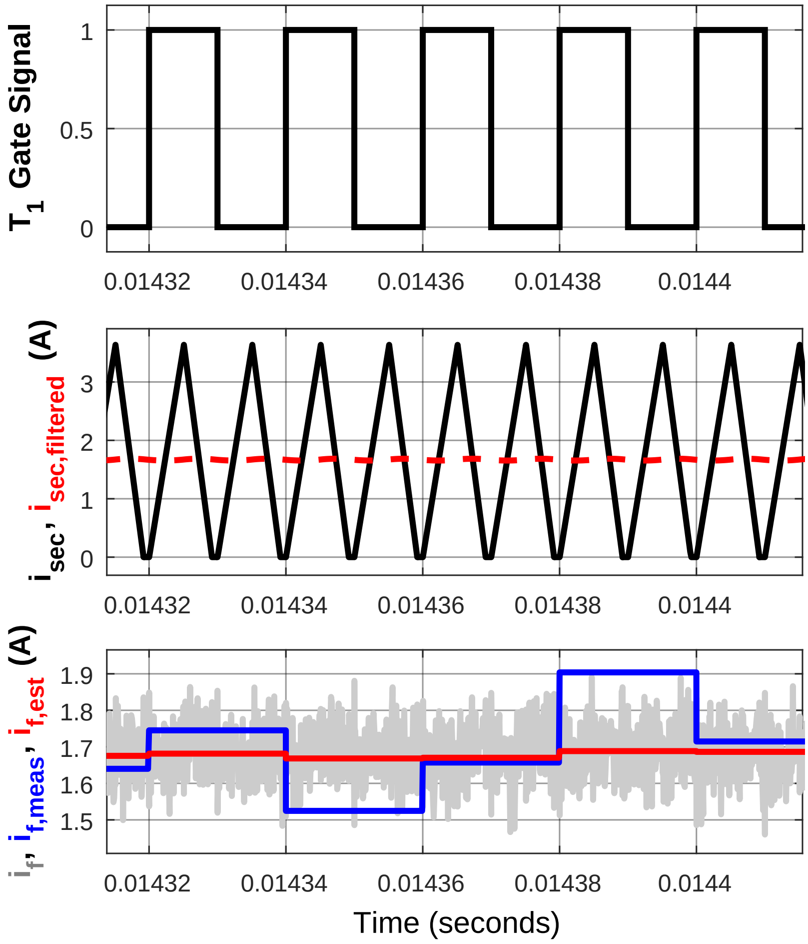

Figure 2.11: Secondary side output current (i_{sec}), real rectified-filtered-scaled primary current (i_f), its measurement ($i_{f,meas}$) and estimation ($i_{f,est}$) where current sampling instants corresponds to rising edge of T_1 gate signal

In the simulation scenario, the output load resistance changes in a piece-wise constant manner. Figure 2.12 shows the output load resistance trajectory according to the designed scenario and output voltage response to disturbances for actual (directly measured) feedback and estimated feedback cases. Since a controller design is not in the main scope of this study, we use a simple Proportional-Integral (PI) voltage controller. We tune the controller for the case where the output voltage feedback is directly available and use the same PI coefficients for the estimated feedback case.

One can see that there exist negligible differences in transient response characteristics between the two cases.

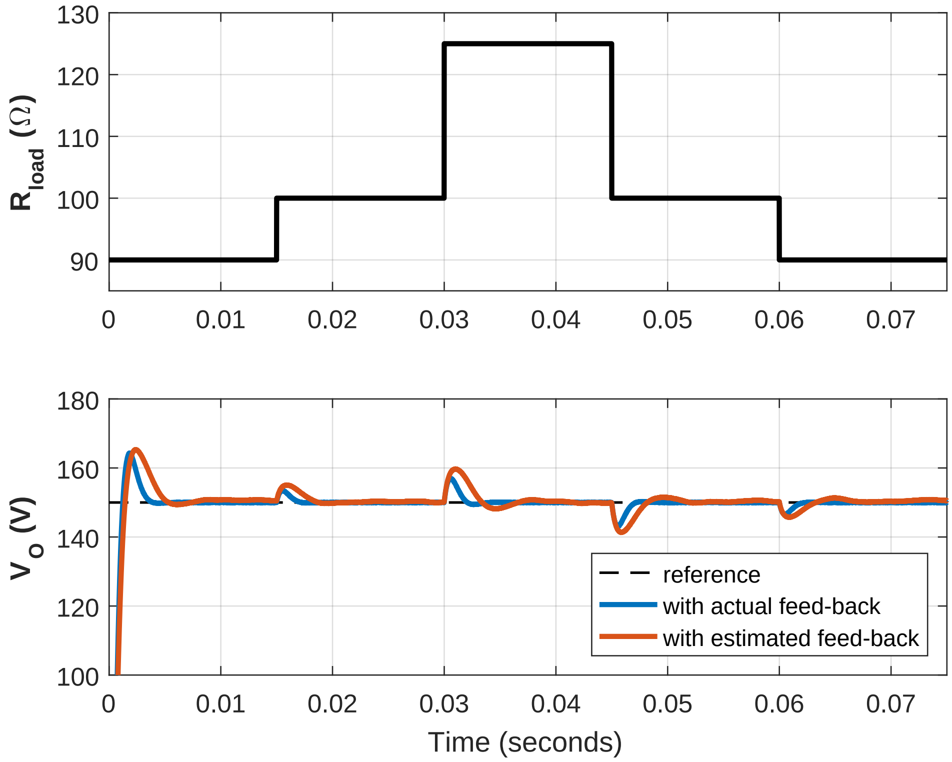

Figure 2.12: Load resistance (R_{load}) and output voltage (V_O) waveforms where the same controller coefficients are used for both actual feedback (V_O) and estimated feedback ($V_{O,est}$) cases

One of the critical design parameters is the variance for the load conductance change (g). As we stated before, the algorithm needs an artificial noise term for this parameter estimation. Since the parameter uncertainty in the load resistance does not fit the Kalman equation's fundamental assumption of zero-mean white Gaussian noise, choosing the appropriate artificial variance ($Q_g = Q(3,3)$) is a design challenge. Figure 2.13 illustrates that, as Q_g increases, bandwidth of observation increases but it brings noise not just for g estimation but also for the other states. Trading-off between noise and bandwidth, we select the variance as $Q_g = 10^{-9}$.

For the sake of practicality, after rectification of the primary current (i_{pri}) we use a 1^{st} order Low-Pass Filter (LPF) which can be implemented by a simple RC filter in the

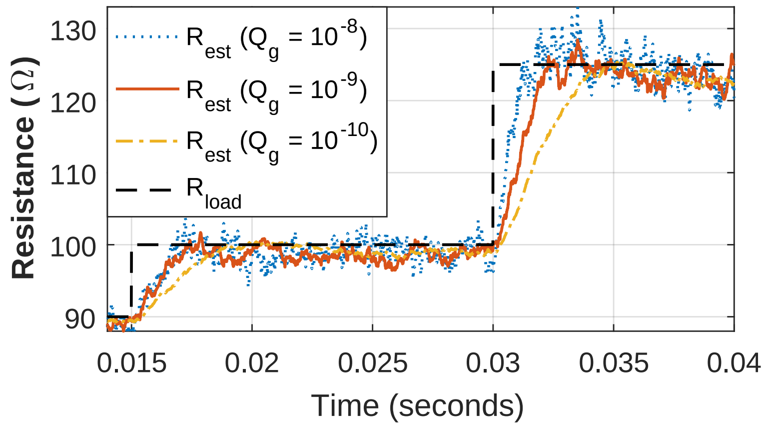

Figure 2.13: Real load resistance (R_{load}) and its estimations (R_{est}) for different variances ($Q_g = Q(3,3)$)

hardware. On the other hand, the unremovable nonlinearities in the simulated circuit causes a small steady-state error in the output voltage estimation. One can see from Figure 2.14 that the cut-off frequency of the current filter can be selected such that it can reduce the steady-state error caused by the nonlinearities. Regarding this effect, we choose the cut-off frequency (f_c) as $1kHz$ comparing with the others on the given plot.

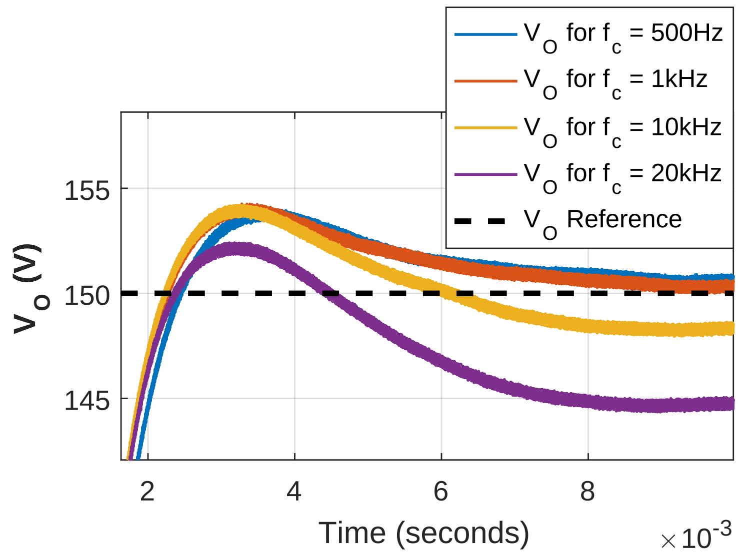

Figure 2.14: Output voltage (V_O) for different low-pass filter cut-off frequencies (f_c) (Here, estimated output voltage $v_{O,est}$ is used as feedback)

Figure 2.15 details the waveforms for the full scenario, which consists of the start-up and two different loads step up and down. Both Figure 2.12 and Figure 2.15 show that the proposed observer can filter out the measurement noise of the current and accurately estimate the total output load resistance and, more importantly, the output voltage. Also, we show that the estimated voltage can be used in a feedback control system directly without changing the controller coefficients.

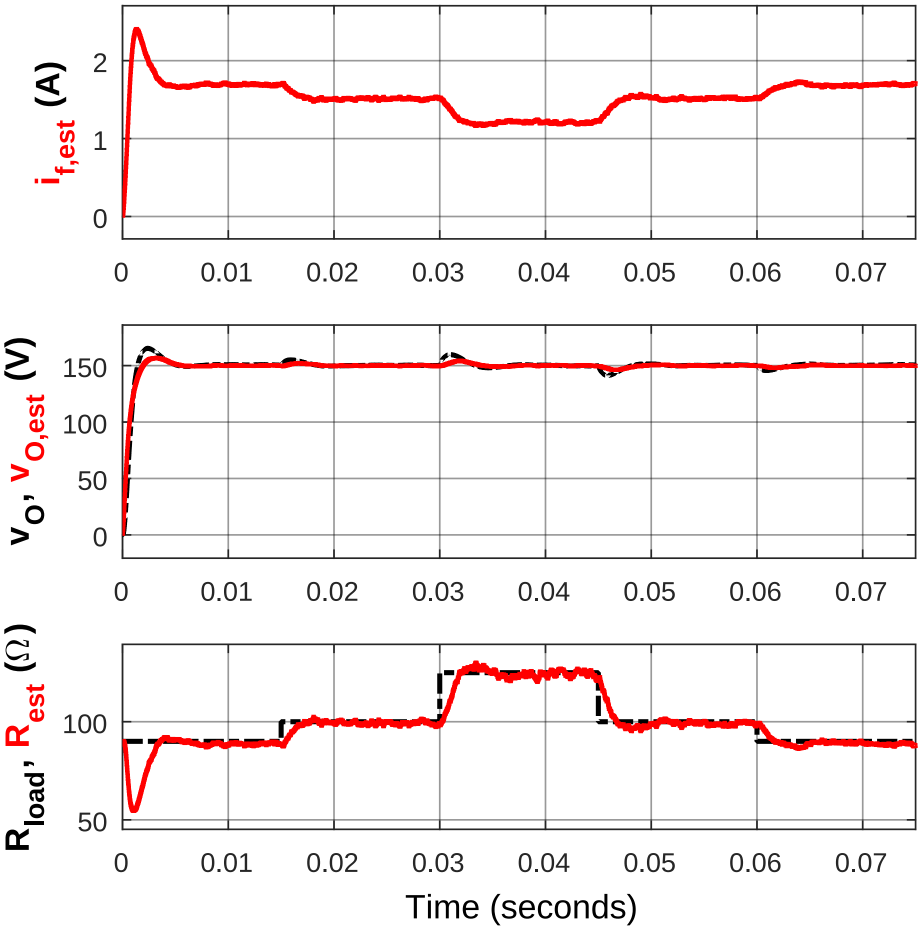

Figure 2.15: Waveforms for estimation of secondary side output current mean ($i_{f,est}$), real output voltage (v_O) and its estimation ($v_{O,est}$), real load resistance (R_{load}) and its estimation (R_{est}) (Here, $v_{O,est}$ is used as feedback)

CHAPTER 3

EXTENDED KALMAN FILTER BASED STATE AND PARAMETER ESTIMATION METHOD FOR A BUCK CONVERTER OPERATING IN A WIDE LOAD RANGE

3.1 Dissemination

Some of the work, figures and text presented in Chapter 3 has been reported in a conference paper [19].

3.2 Introduction

Due to its low-cost and robustness, Buck converter topology (see Figure 3.1) is very common in modern industrial power supplies and it exhibits well-known steady-state and dynamic properties [7–9, 38–42]. Throughout years researchers extensively analyzed the steady-state and dynamic properties of these circuits and developed different design and synthesis approaches [3, 6, 43–47]. Indeed, due to rapid change in flow between CCM and DCM, the Buck converter's behavior corresponds to a hybrid dynamical system. Thus, the control problem of a one quadrant Buck converter over a wide load range is not straightforward. Moreover, the Buck converter topology blocks the reverse power flow, which means that it is impossible to reduce a rapid increase in the output voltage actively. Thus, avoiding or at least limiting overshoots of the output voltage becomes crucial for this topology [37].

The development of a suitable mathematical model capturing the plant system's important dynamics is the starting point for the converter controller design. Researchers have proposed different small-signal and large-signal modeling approaches to de-

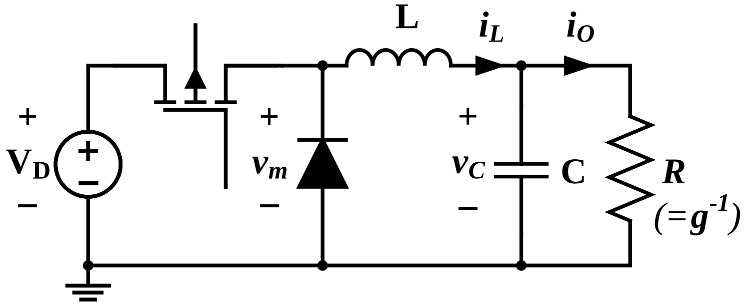

Figure 3.1: Circuit diagram of the Buck converter

scribe the dynamics of the Buck converter [7, 8, 38–42]. The most preferred and conventional modeling approach for Buck converter topology is the state-space averaging. Under this modeling framework, the Buck converter shows a linear second-order characteristic in CCM [7, 8], on the other hand, it exhibits nonlinear first-order system dynamics in DCM [9].

The most common and most straightforward control policy used for Buck converters is the PID voltage regulator. Typical control design and tuning procedures dominantly rely on small-signal models. In that respect, it is fair to claim that these models are only "valid" around a particular operating point [6]. Moreover, the resultant closed-loop control systems can be non-robust or sub-optimal when the behavior deviates from the nominal range due to unknown changes in the load resistance. Thus, this simple control structure does not guarantee stable and well-behaved dynamics for broad operating range applications [44]. Researchers propose alternative control algorithms to remedy these problems, taking into account the load-dependent dynamics [45, 46]. However, since they do not consider the change in the system dynamics, which occurs due to operation mode change in between CCM and DCM, these propositions are not appropriate for a general design approach.

Similar to our attempt in this study, Broeck et al. [37], propose a unified control structure of a Buck converter that can also operate in wide load range applications, where a nonlinear predictive observer estimates the inductor current and output voltage. The algorithm in [37] updates the active controller structure based on the predictions on the mode of operation. However, they do not explicitly model or incorporate the unavoidable process and measurement noises that are inevitable in real-life applications.

In our approach in this study, we explicitly integrate the process and measurement noise in our design phase. Specifically, we propose an observer based on the Extended Kalman Filter, which can estimate the system states (capacitor voltage and inductor current) and unknown parameters such as load resistance, as well as predict the operation mode of the model explicitly integrating the process and measurement noise. EKF is the most common extension of the Kalman Filter to nonlinear systems. The EKF algorithm uses the original nonlinear equations for state projection & measurement residual computation phases (See Figure 3.4). However, it linearizes all other nonlinear transformations and substitutes Jacobian matrices for the linear transformations in the Kalman Filter equations by exploiting the assumption that instantaneous dynamics are quasi-linear [14, 48–50]. We presented the large-signal modeling of the converter for CCM and DCM separately, and we demonstrated the designed observer performance in MATLAB Simulink environment.

3.3 Modeling of the Converter

Throughout the modeling, for the Buck converter circuit depicted in Figure 3.1 we assume that transistor and diode are ideal components, output load is resistive and we ignore ESR of capacitor C and DCR of inductor L.

Operating point independent model development is very important to comprehend the dynamic characteristics of Buck converter over a wide operating range. Due to change in operation mode for wide load range applications of Buck converter, it is not possible to use one single model for the entire load range. Moreover, vast majority of modern control and estimation applications in industrial electronics use digital controllers. For these reasons, in this study we derived discrete-time dynamic models for CCM and DCM separately. Figure 3.2 depicts the sampling instants during discretizing the dynamics of two modes of operation. In this context, we utilize the models based on the difference equations of the Buck converter [37].

Switching ON and OFF the transistor in Figure 3.1, we apply PWM voltage v_{pwm} at the input of LC filter. If the inductor current i_L does not decay to zero over one PWM interval, this corresponds to CCM operation where we can model the dynamics of

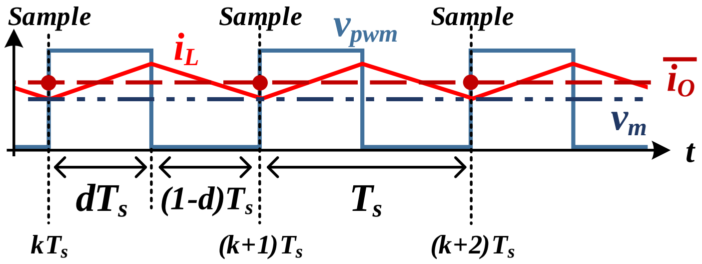

(a)

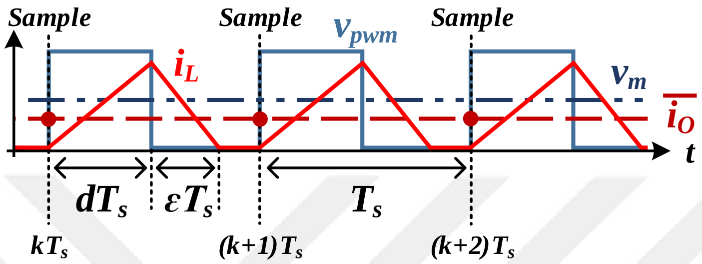

(b)

Figure 3.2: PWM voltage (v_{pwm}), manipulated voltage (v_m), inductor current (i_L) and sampling of output current (i_O) waveforms for (a) CCM and (b) DCM operation of the Buck converter

the system by applying the large-signal state-space averaging technique [42]. Hence, we can average all the states over one sampling interval of T_s. We call the average reverse voltage across the diode within one switching cycle as manipulated voltage (v_m) which is expressed as follows

$$v_m(t) = \frac{1}{T_s}\int_{kT_s}^{(k+1)T_s} v_{pwm}(\tau)d\tau = d(kT_s)V_D \tag{3.1}$$

Since LC filter has low-pass characteristics, we can tolerate the averaging. We describe the dynamics of the LC filter as a function of the manipulated voltage (v_m) and load conductance (g) as given in equations (3.2) and (3.3).

$$L\frac{d}{dt}i_L(t) = v_m(t) - v_C(t) \tag{3.2}$$

$$C\frac{d}{dt}v_C(t) = i_L(t) - v_C(t)g(t) \tag{3.3}$$

In the model expressions, we use characteristic impedance and resonant frequency parameters of the effective LC filter given as

$$Z_0 = \sqrt{L/C} \tag{3.4}$$

$$\omega_0 = \frac{1}{\sqrt{LC}} \tag{3.5}$$

We further assume that the sampling frequency is equal to switching frequency and in the following subsections we present the derivation of the system equations ($x_{k+1} = f_k(x_k, u_k, 0)$) for CCM and DCM.

3.3.1 CCM Discrete-Time Modeling

In CCM operation, assuming constant manipulated voltage (v_m) and load current (i_O) over one switching period, we can solve the differential equations (3.2) and (3.3) with initial conditions. Inductor current (i_L) and capacitor voltage (v_C) can be obtained as functions of the initial conditions as follows,

$$\begin{aligned} i_L(t) = &\frac{1}{Z_0}sin(\omega_0 t)(v_m(0) - v_C(0)) + \cdots \\ &\cdots + cos(\omega_0 t)i_L(0) + (1 - cos(\omega_0 t))v_C(0)g(0) \end{aligned} \tag{3.6}$$

$$\begin{aligned} v_C(t) = &(1 - cos(\omega_0 t))v_m(0) + \cdots \\ &\cdots + Z_0 sin(\omega_0 t)(i_L(0) - v_C(0)g(0)) + \cdots \\ &\cdots + cos(\omega_0 t)v_C(0) \end{aligned} \tag{3.7}$$

Equations (3.4), (3.5), (3.6) and (3.7) can be used to derive the difference equations showing the inductor current and capacitor voltage evolution at one sampling time span (T_s). Since it is easier to calculate the partial derivatives, we use load conductance ($g = 1/R$) instead of the resistance (R). So, the resultant discretized augmented model for CCM takes the form in (3.8).

$$f_{k,CCM} = x_{k+1} = \begin{bmatrix} i_L[k+1] \\ v_C[k+1] \\ g[k+1] \end{bmatrix} = \cdots$$
$$\cdots \begin{bmatrix} i_L[k]cos(\omega_0 T_s) + v_C[k](-\frac{sin(\omega_0 T_s)}{Z_0}) + v_C[k]g[k](1 - cos(\omega_0 T_s)) \\ i_L[k](Z_0 sin(\omega_0 T_s)) + v_C[k](cos(\omega_0 T_s)) + v_C[k]g[k](-Z_0 sin(\omega_0 T_s)) \\ g[k] \end{bmatrix} + \cdots \tag{3.8}$$
$$\cdots + \begin{bmatrix} \frac{sin(\omega_0 T_s)}{Z_0} \\ 1 - cos(\omega_0 T_s) \\ 0 \end{bmatrix} v_m[k]$$

3.3.2 DCM Discrete-Time Modeling

We assume that the resonant frequency of the LC filter is lower than the sampling frequency ($\omega_0 T_s \ll 1$) and system takes samples at the beginning of each PWM interval where the discontinuous inductor current is zero. Solving the continuous time differential equations for inductor (L) and capacitor (C) we obtain

$$v_C(t) \approx v_C(0) + (i_L(0) - v_C(0)g(0))Z_0\omega_0 t \tag{3.9}$$

$$i_L(t) \approx i_L(0) + (v_m(0) - v_O(0))\frac{\omega_0}{Z_0}t \tag{3.10}$$

Table 3.1 shows the characteristic instances of the current and voltage signals during one PWM period in DCM operation. Note that the equations are written in terms of output load current $i_O(t)$ which is actually equal to $v_C(t)g(t)$.

We use these approximated equations to come up with the dynamics of the converter in DCM over one period. The calculation point is at the instant when we switch ON the transistor. During the active voltage pulse (dT_s duration), the current i_L increases

Table 3.1: Buck Converter Inductor Current and Capacitor Voltage at the Characteristic Instances During One Pulse Width Modulation Period in Discontinuous Conduction Mode

$\mathbf{t_X}$	$\mathbf{v_C(kT_s + t_X) =}$	$\mathbf{i_L(kT_s + t_X) =}$
$t_X = dT_s$	$v_C(kT_s) -$ $i_O(kT_s)Z_0\omega_0 dT_s$	$(V_D - v_C(kT_s))\frac{dT_s\omega_0}{Z_0}$
$t_X = (d+\varepsilon)T_s$	$v_C(kT_s)(1-(\omega_0T_s)^2 d\varepsilon) -$ $Z_0\omega_0T_s(\varepsilon + d)i_O(kT_s) +$ $(\omega_0T_s)^2(d\varepsilon)V_D$	0
$t_X = T_s$	$v_C(kT_s)(1-(\omega_0T_s)^2 d\varepsilon) -$ $Z_0\omega_0T_s i_O(kT_s) +$ $(\omega_0T_s)^2(d\varepsilon)V_D$	0

up to its peak value in (3.11).

$$i_L(kT_s + dT_s) = (V_D - v_C(kT_s))\frac{dT_s\omega_0}{Z_0} \tag{3.11}$$

After dT_s time span, inductor current decays to zero. We need the current decay time (ε) given in (3.12) to calculate the output capacitance voltage in (3.13) at the end of the PWM interval.

$$\varepsilon(kT_s) = \frac{(V_D - v_C(kT_s))d(kT_s)}{v_C(kT_s) - Z_0\omega_0T_s d(kT_s)v_C(kT_s)g(kT_s)} \tag{3.12}$$

$$\begin{aligned} v_C((k+1)T_s) &= v_C(kT_s) - Z_0\omega_0T_s v_C(kT_s)g(kT_s) + \cdots \\ &\cdots + \frac{d(kT_s)^2(\omega_0T_s)^2(V_D - v_C(kT_s))^2}{v_C(kT_s) - Z_0\omega_0T_s d(kT_s)v_C(kT_s)g(kT_s)} \end{aligned} \tag{3.13}$$

Arranging the expressions we end up with the augmented model in equation (3.14) as

DCM model where $d[k]$ is duty cycle of PWM.

$$
\begin{aligned}
f_{k,DCM} = x_{k+1} = \begin{bmatrix} i_L[k+1] \\ v_C[k+1] \\ g[k+1] \end{bmatrix} = \cdots \\
\cdots \begin{bmatrix} 0 \\ v_C[k] - v_C[k]g[k](Z_0\omega_0 T_s) + \frac{d[k]^2(\omega_0 T_s)^2(V_d[k]-v_C[k])^2}{v_C[k]-v_C[k]g[k]d[k](Z_0\omega_0 T_s)} \\ g[k] \end{bmatrix}
\end{aligned}
\tag{3.14}
$$

3.4 Extended Kalman Filter Based State and Parameter Estimator Design

Figure 3.3 illustrates the proposed observer design that we developed for a Buck converter control. We have obtained 3^{rd} order and 2^{nd} order non-linear discrete-time models for CCM and DCM, respectively in Sec. 3.3. Here, we use the discrete-time EKF to observe the actual output capacitor voltage (v_C), inductor current (i_L) and estimate the load resistance or conductance (R or g) as well as the operation mode of the system ($mode$) from noisy capacitor voltage ($v_{C,meas}$) and output load current ($i_{O,meas}$) measurement in an environment with process noise. The proposed algorithm updates the load resistance estimation (as well as system states) in real-time. In this context, one can detect the mode by comparing estimated load resistance (R_{est}) with critical resistance ($R_{critical}$) [3]. However, considering the overshoots and settling time in estimation of the load resistance, we use a different method for faster mode detection. We check the CCM estimation $v_{C,est,CCM}$ in a predetermined band where we compare $v_{C,est,CCM}$ with $v_{C,meas}(1 \pm \alpha)$ at each PWM cycle. The mode is estimated according to following equation

$$
\begin{aligned}
&mode_k = \\
&\begin{cases} \text{CCM}, & if \;\; v_{C,est,CCM} \in (v_{C,meas}(1-\alpha), v_{C,meas}(1+\alpha)) \\ \text{DCM}, & Otherwise \end{cases}
\end{aligned}
\tag{3.15}
$$

Here, mode band coefficient ($\alpha \in (0,1)$) is a design parameter affecting the mode

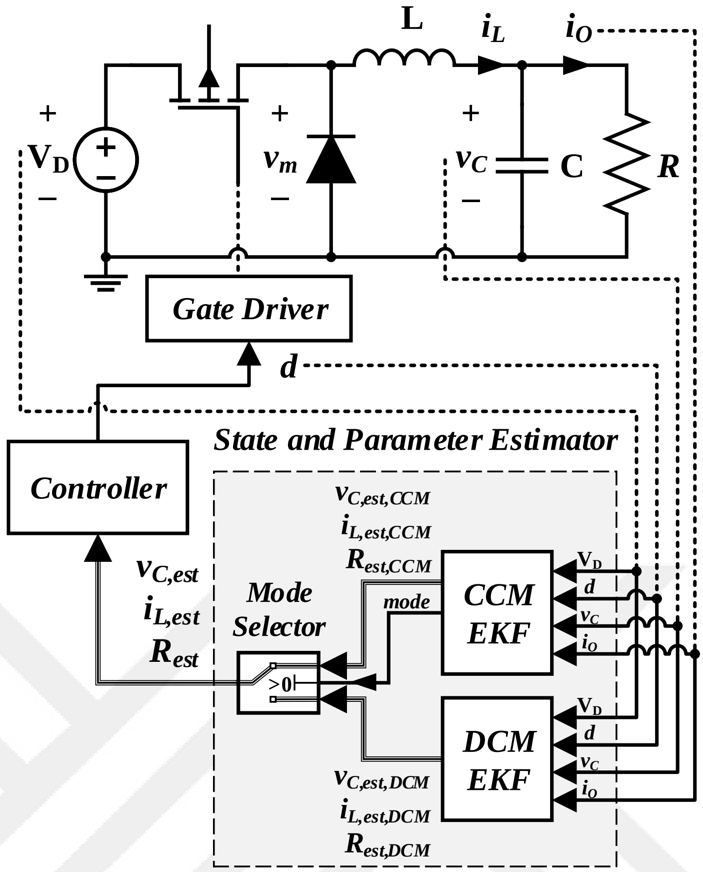

Figure 3.3: Diagram of the proposed EKF-based observer utilization for Buck converter voltage control

detection performance in terms of estimation errors during transitions in between modes. This method is based on the fact that CCM EKF capacitor voltage estimation deviates from the actual value when the converter operates in DCM. On the other hand, DCM EKF accurately estimates the voltage on the entire operating range. Certainly, filtering performances of each EKF block has better results for their own regions. Utilizing this fact and selecting an appropriate α, the proposed method estimates the mode using equation (3.15).

Figure 3.4 details the EKF algorithm for a generic non-linear discrete-time state-space model where hat symbol $(\hat{.})$ denotes estimate, plus superscript $(.^{+})$ denotes *a posteriori* (after we process the measurement) and minus superscript $(.^{-})$ denotes *a priori* (before we process the measurement) along with state (x_k) and error covariance (P_k) at sub-scripted time k.

Dynamic System Equations

$$
\begin{aligned}
x_k &= f_{k-1}(x_{k-1}, u_{k-1}, \omega_{k-1}) \\
y_k &= h_k(x_k, v_k) \\
\omega_k &\sim (0, Q_k) \\
v_k &\sim (0, R_k)
\end{aligned}
$$

Initialization

$\hat{x}_o^+$ *and* P_0^+

For $k = 1,2,\cdots$

Prediction

1. State projection (*a priori* state estimate)

$$\hat{x}_k^- = f_{k-1}(\hat{x}_{k-1}^+, u_{k-1}, 0)$$

2. Error covariance projection

$$P_k^- = F_{k-1} P_{k-1}^+ F_{k-1}^T + L_{k-1} Q_{k-1} L_{k-1}^T$$

Correction

1. Kalman gain computation

$$K_k = P_k^- H_k^T \left(H_k P_k^- H_k^T + M_k R_k M_k^T \right)^{-1}$$

2. Estimation update with measurement y_k (*a posteriori* state estimate)

$$\hat{x}_k^+ = \hat{x}_k^- + K_k [y_k - h_k(\hat{x}_k^-, 0)]$$

3. Error covariance update

$$P_k^+ = (I - K_k H_k) P_k^-$$

where $F_{k-1} = \frac{\partial f_{k-1}}{\partial x}|_{\hat{x}_{k-1}^+}$, $L_{k-1} = \frac{\partial f_{k-1}}{\partial \omega}|_{\hat{x}_{k-1}^+}$

and $H_k = \frac{\partial h_k}{\partial x}|_{\hat{x}_k^-}$, $M_k = \frac{\partial h_k}{\partial v}|_{\hat{x}_k^-}$

Figure 3.4: Discrete-time Extended Kalman Filter (EKF) algorithm

Simulations show that this approach can accurately detect the mode of the system. Both CCM EKF and DCM EKF algorithms run at the same time and the mode selector outputs the estimations according to the currently detected mode.

3.5 Controller Design

We use PID voltage controller in this application and we select the controller parameters based on the discrete time model. We compare overshoot and settling time performances of the responses and we select the best option.

Figure 3.5 shows open loop bode diagram (from duty cycle to output voltage) of the discrete-time converter system for nominal maximum and minimum output load resistances ($R = 90\Omega$ and $R = 900\Omega$).

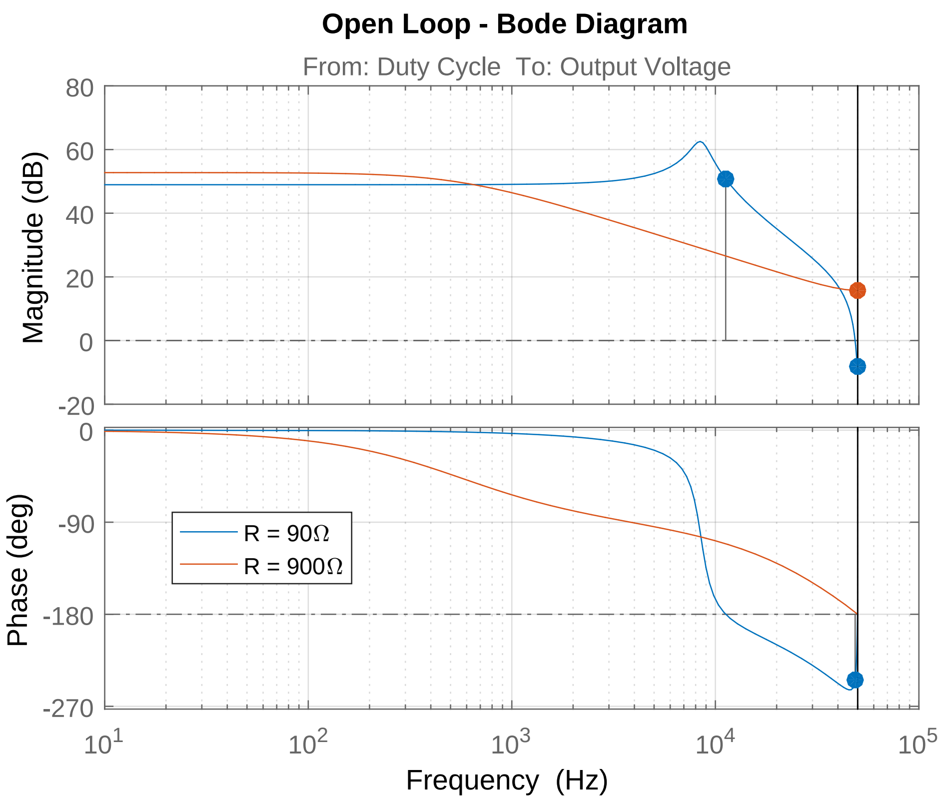

Figure 3.5: Open loop bode diagram of the discrete-time Buck converter system for maximum and minimum load conditions. Here, gain margin is $-64.3dB$ at frequency of $48.6kHz$ and the system is not stable.

Since controller design is not in the main scope of this study, investigating the open loop bode plot, we decide to use just a PI voltage controller. For different crossover frequencies, we tune PI coefficients for better disturbance rejections and reference tracking. Figure 3.6 shows step responses for different PI controllers and Table 3.2 gives corresponding coefficients and details of these responses.

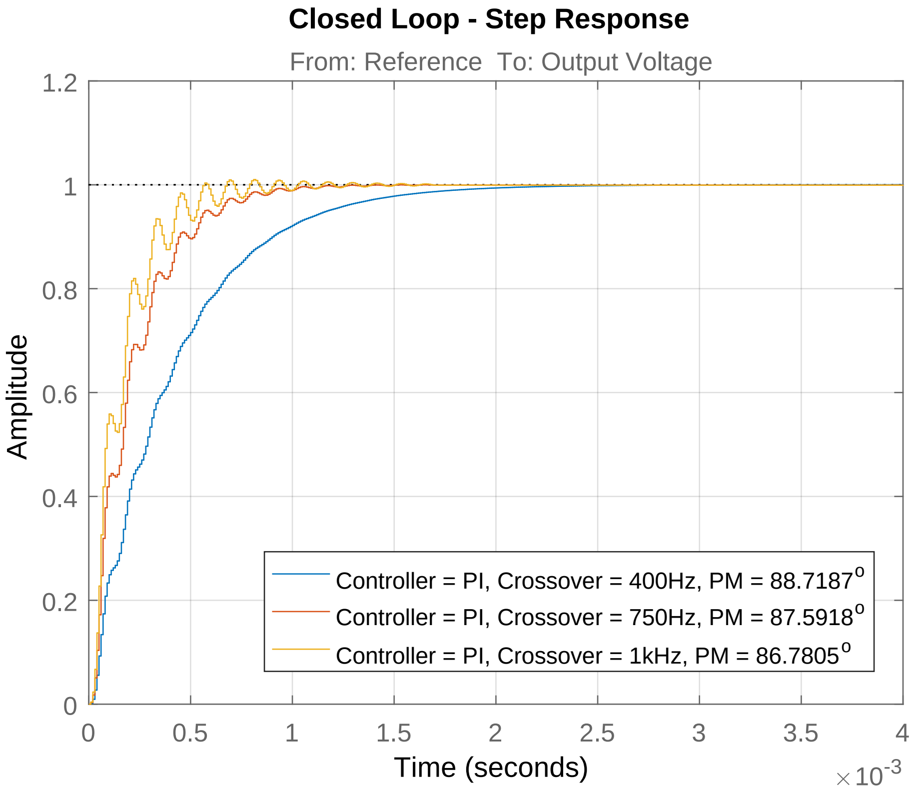

Figure 3.6: Step responses of the discrete-time Buck converter system for different PI controllers

Table 3.2: Controller Options for Buck Converter System

K_P	K_I	T_s (sec)	Crossover Frequency (Hz)	Phase Margin $(^o)$	Overshoot $(\%)$	Settling Time $(msec)$
4.48×10^{-5}	8.96	1×10^{-5}	400	88.7187	0	1.530
8.35×10^{-5}	16.7	1×10^{-5}	750	87.5918	0.00484	0.867
0.000111	22.1	1×10^{-5}	1000	86.7805	1.02	0.764

We select the 2^{nd} controller in Table 3.2 considering both overshoot and settling time performances.

Figure 3.7 shows controlled system bode diagram for the following PI coefficients:

$$\begin{aligned} K_P &= 8.35 \times 10^{-5}\,, \\ K_I &= 16.7\,, \\ T_s &= 1 \times 10^{-5}\,. \end{aligned} \tag{3.16}$$

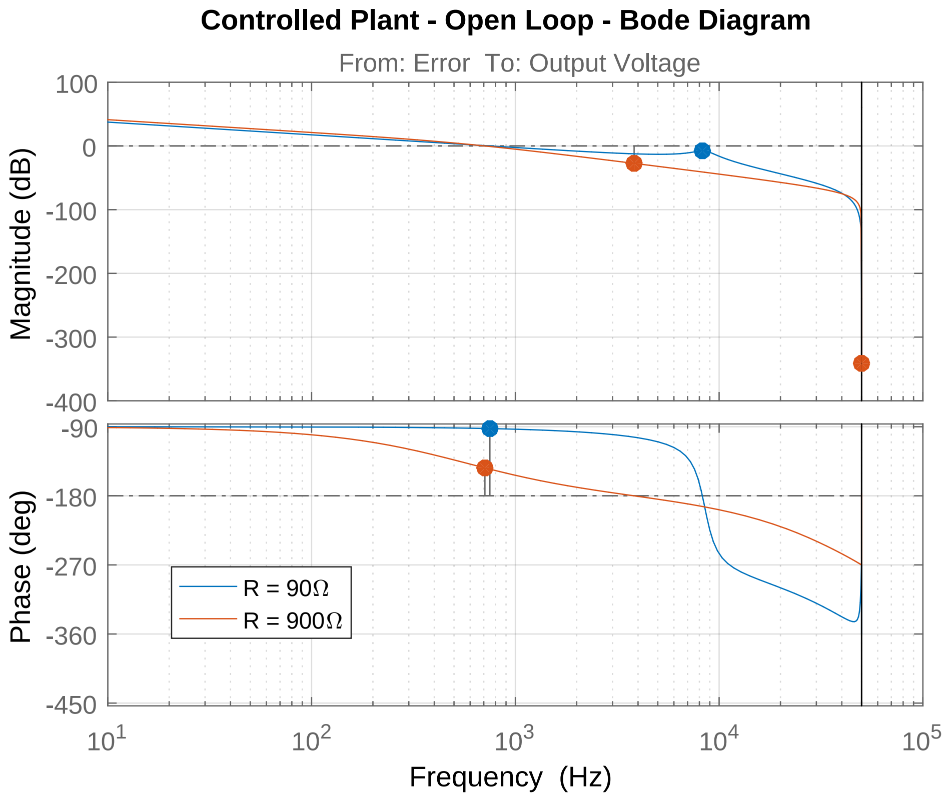

Figure 3.7: Bode diagram of the controlled discrete-time Buck converter system with selected PI controller. Here, for $R = 90\Omega$ phase margin is $87.6dB$ at frequency of $750Hz$ and the system is stable. Also, for $R = 900\Omega$ phase margin is $36.4dB$ at frequency of $706Hz$ and the system is stable.

3.6 Simulation Results

For the simulation studies, we assume that we know the process and measurement noise co-variances (Q_k and R_k) apriori except load conductance (g) variance. We describe the determination of g variance ($Q_g = Q_k(3,3)$) and mode band coefficient (α) in this section. We provide the simulated converter circuit and EKF parameters in Table 3.3.

Table 3.3: Simulated Circuit Parameters, Process and Measurement Noise Co-variances for the Buck Converter Study

Input voltage	V_D = 280 V
Output voltage	V_O = 150 V
Output power	P_O = 25-250 W
Filter inductance	L = 350 μH
Filter capacitance	C = 1 μF
Switching frequency	f_s = 100 kHz
Process noise co-variance	$Q_k = \begin{pmatrix} 10^{-4} & 0 & 0 \\ 0 & 10^{-3} & 0 \\ 0 & 0 & 10^{-10} \end{pmatrix}$
Measurement noise co-variance	$R_k = \begin{pmatrix} 5 \times 10^{-3} & 0 \\ 0 & 1 \end{pmatrix}$
Mode band coefficient	α = 0.1

Even though the change in the load resistance (R) trajectories are deterministic in the simulation scenario, the EKF algorithm still needs a small artificial noise term allowing the Kalman Filter to change its estimate of the parameter [14]. We accept all the required assumptions given at the beginning of Sec. 3.3 and simulate the Buck converter and estimation algorithm in MATLAB Simulink environment. Instead of an average model, we simulate the circuit using *Simscape/Power Systems/Specialized Technology* library in Simulink, which brings unmodeled effects such as transistor resistance, diode resistance, and forward voltage. Although this implies that the simulated Buck converter is not ideal as stated in the modeling part, simulation results show that we can use this method even in the presence of unmodeled and potentially nonlinear dynamic uncertainties. Figure 3.8 illustrates how we integrate the process and measurement noises to current and voltage states inside the converter circuit simulation.

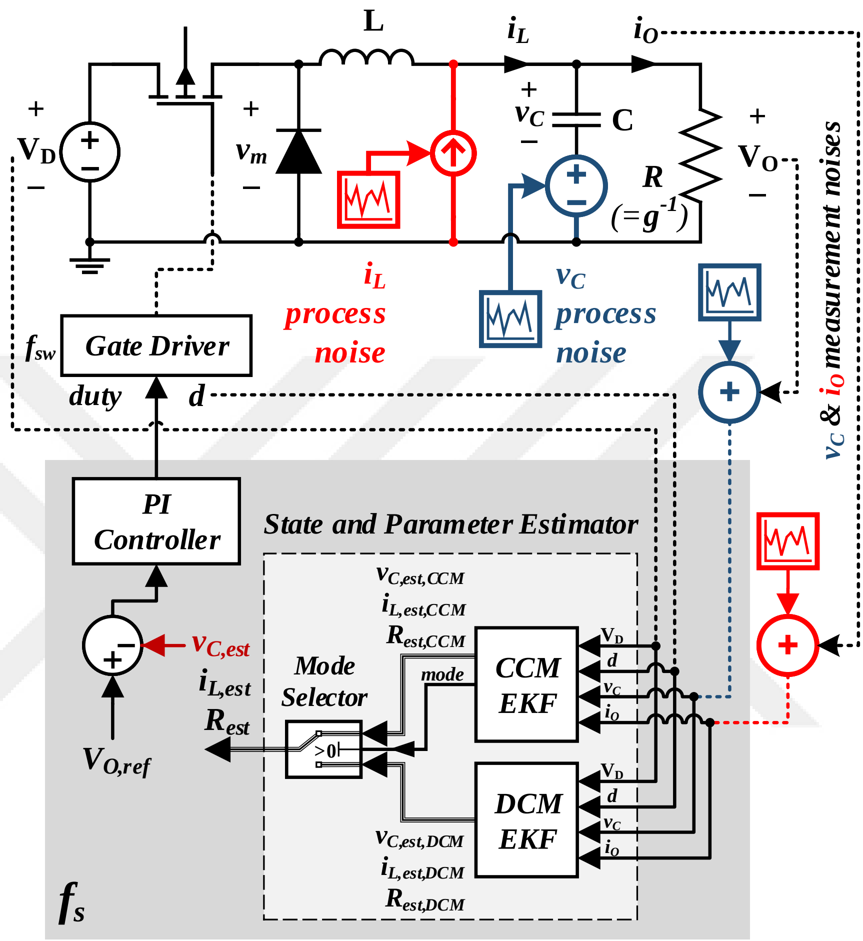

Figure 3.8: Simulation environment diagram showing process and measurement noise addition to signals

In the simulation scenario, the output load resistance changes in a piece-wise constant manner. Figure 3.9 shows the output load resistance trajectory according to the designed scenario and output voltage response to disturbances for actual (directly measured) feedback. Since a controller design is not in the main scope of this study, we adopt a simple Proportional-Integral (PI) voltage controller for the simulation in Figure 3.9 and use the same PI controller coefficients for the estimated voltage feedback case in Figure 3.8.

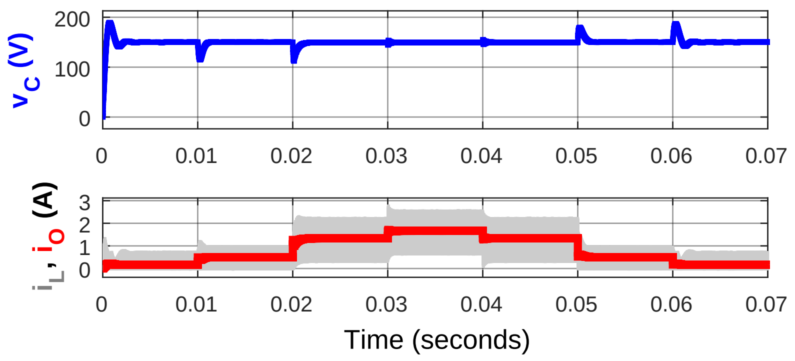

Figure 3.9: Output voltage (v_C), inductor and load current (i_L and i_O) responses to load change

As we discussed in Sec. 3.3, our method sample the signals at the end of each PWM period to capture the dynamics in DCM operation where the inductor current is zero. As an example, Figure 3.10 shows a continuous inductor current sampling.

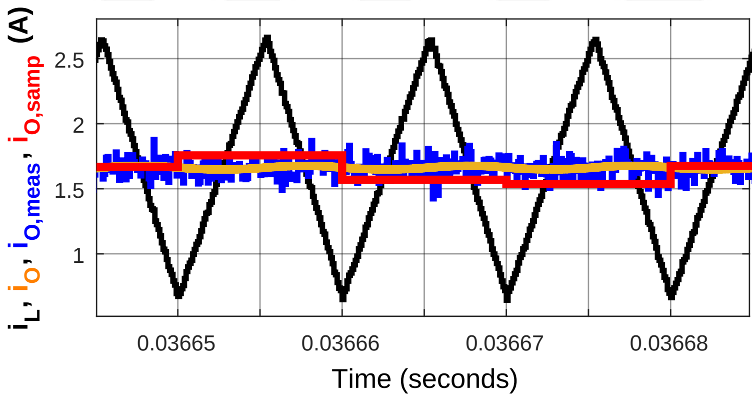

Figure 3.10: Inductor current (i_L), output load current (i_O), its measurement ($i_{O,meas}$) and taken sample ($i_{O,samp}$)

One of the critical design parameters in our approach is the variance of the load conductance (g). As we stated before, the algorithm needs an artificial noise term for the estimation of this parameter. Since, the parameter uncertainty in the load resistance does not fit the Kalman equation's fundamental assumption of zero-mean white Gaussian noise, choosing the appropriate artificial variance ($Q_g = Q_k(3,3)$) is a design challenge. In this study, we tuned this parameter by a simple trial and error approach. As Q_g increases, the bandwidth of observation increases, but it brings noise not just for g estimation but also for the other states. Trading-off between noise and bandwidth, we select the variance as $Q_g = 10^{-10}$.

We determined the so-called mode band coefficient (α) on simulation experiments. Increasing α results in longer settling times and decreasing it causes glitches in the mode detection. Considering these, we determined the value for the given simulation scenario as $\alpha = 0.1$.

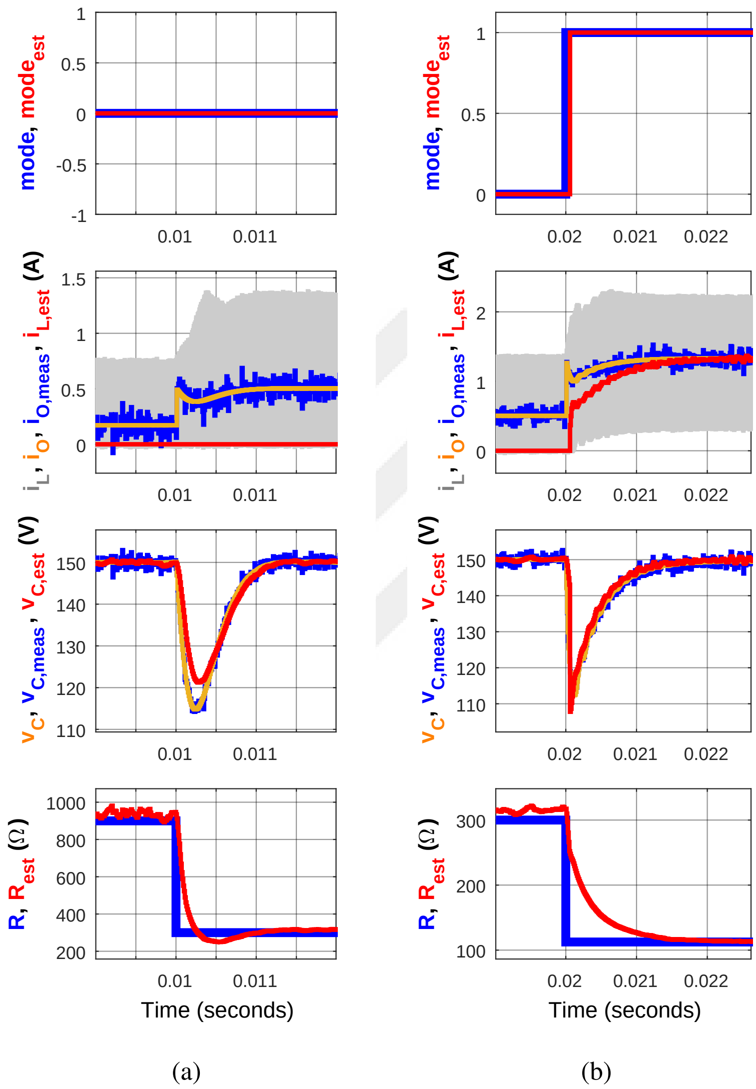

Figure 3.11: Simulation results showing mode estimation ($mode_{est}$), inductor current estimation ($i_{L,est}$), capacitor voltage estimation ($v_{C,est}$) and load resistance estimation (R_{est}) with respect to actual values for the transitions in between same and different modes of operation (a) DCM to DCM, (b) DCM to CCM

In order to evaluate the steady-state performance of the estimation, we use the Nor-

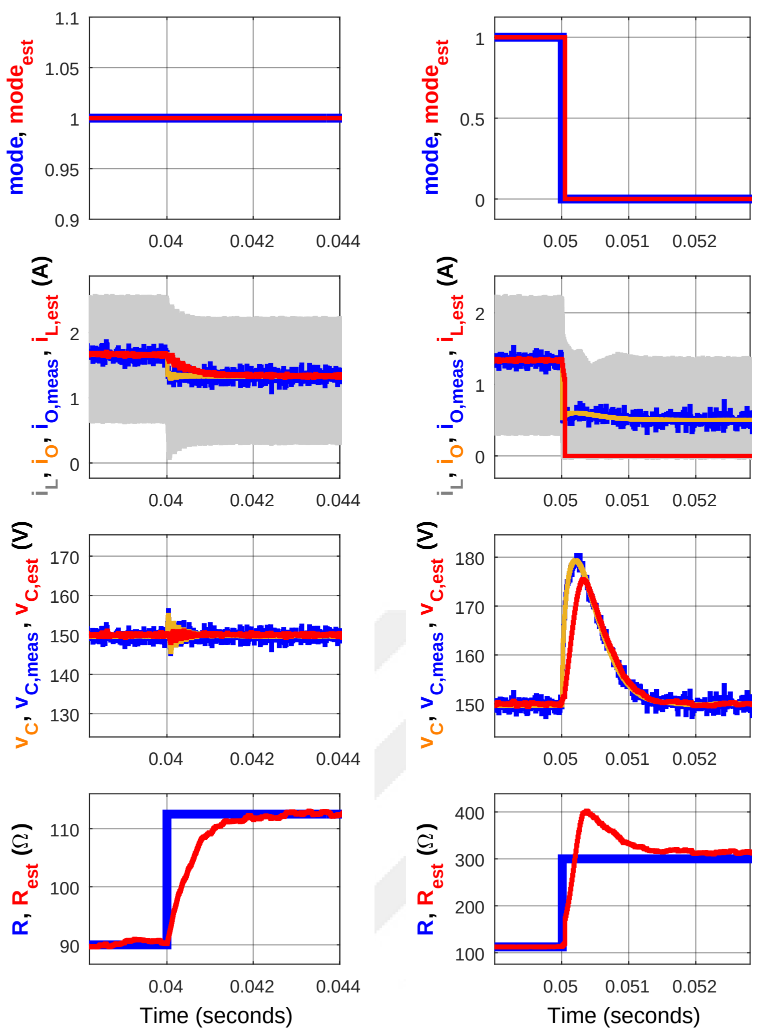

(a) (b)

Figure 3.12: Simulation results showing mode estimation ($mode_{est}$), inductor current estimation ($i_{L,est}$), capacitor voltage estimation ($v_{C,est}$) and load resistance estimation (R_{est}) with respect to actual values for the transitions in between same and different modes of operation (a) CCM to CCM, (b) CCM to DCM

malized Root-Mean-Square Deviation (NRMSD) for different regions. Note that, according to the discrete-time model, the inductor current state is zero. This is why $NRMSD(i_L)$ for DCM regions become 0%.

$$NRMSD(x) = \frac{\sqrt{\frac{\sum_{i=1}^{T}(x_{error,i})^2}{T}}}{\overline{x_{actual}}} \tag{3.17}$$

Table 3.4 details the NRMSD values for different steady-state regions and Figure 3.11 and Figure 3.12 illustrates the estimation results for the transitions between the same and different modes in the given scenario.

Table 3.4: Normalized Root-Mean-Square Deviations for the Buck Converter Simulation Study

	Heavy DCM	Light DCM	Light CCM	Heavy CCM
$NRMSD(i_L)$	0%	0%	1.32%	0.99%
$NRMSD(v_C)$	0.47%	0.67%	0.67%	0.67%
$NRMSD(R)$	4.7%	5.15%	0.59%	0.34%

Both Table 3.4, Figure 3.11 and Figure 3.12 show that the proposed observer can filter out the measurement noise of the voltage and current and accurately estimate the total output load resistance and, more importantly, the mode of operation with acceptable steady-state and transition performance.

CHAPTER 4

CONCLUSIONS

In this thesis, we investigated utilization of Kalman Filter for different state and parameter estimation problems in DC/DC power electronic converters. We took two different topologies into consideration. Each topology has its specific estimation problem and we proposed convenient methods to these in two separate studies.

4.1 Dissemination

Some part of the text presented in Chapter 4 has been reported in a conference paper [19].

4.2 Conclusion of the Full-Bridge Converter Study

In the first study, we have presented a Linearized Kalman Filter observer-based sensorless voltage control method for a Full-Bridge DC/DC converter. The proposed observer estimates the output voltage and load resistance by using the rectified-filtered-scaled primary current measurement. Simulation results show that the proposed observer operates accurately and robustly, and estimated output voltage feedback provides a stable and comparable transient performance as a closed-loop system with actual measurements.

Our proposed method reduces the number of components effectively since the only measurement instrumentation is a single current sensor that reads the primary current in the whole system. Moreover, our approach decreases the input-output isolation capacitance by removing the voltage sensor in between the sides. The only challenge in the implementation is the tuning and selection of the observer noise co-variances in a hardware platform, specifically the component related to the parameter uncertainty of the load resistance.

In the future, we are planning to integrate formal methods such that the system autotunes models' noise co-variances in a calibration phase. It may also be possible to implement an adaptive noise calibration technique which can continuously monitor and update the noise parameters throughout the operation. Offline and online expectation and maximization techniques can be suitable for these extensions [51–53]. These possible future improvements can further improve the effectiveness and practical adoption of the method in real hardware-based applications.

We believe that this study can guide the development of more robust and high performance sensorless voltage control policies for the Full-Bridge and other isolated DC/DC converter topologies.

4.3 Conclusion of the Buck Converter Study

In the second study, we have presented an EKF based estimation method for a DC/DC Buck converter. The proposed method observes output capacitor voltage and inductor current and estimates the load resistance and detects mode of the system, in an explicit process and measurement noise integrated environment. Simulation results show that the proposed method operates both in CCM and DCM regions accurately and robustly with permissible steady-state NRMSD, transition overshoot, and settling time.

We believe that our state and parameter estimation approaches can guide the development of more robust and high-performance voltage control policies for the Buck converter topology and other DC/DC converter topologies. As future work, we will experimentally verify the proposed estimation method on real converter hardware. We will also implement data-driven statistical determination methods for noise parameters inside the EKF framework.

REFERENCES

[1] N. Mohan, T. M. Undeland, and W. P. Robbins, *Power Electronics: Converters, Applications and Design*. John Wiley and Sons, Inc, third ed., 2003.

[2] R. E. Kalman, "A New Approach to Linear Filtering and Prediction Problems," *Journal of Basic Engineering*, vol. 82, pp. 35–45, 03 1960.

[3] R. W. Erickson and D. Maksimovic, *Fundamentals of Power Electronics*. Springer, 2ed ed., 2001.

[4] D. Zhang, *A Stochastic Approach To Digital Control Design And Implementation In Power Electronics*. PhD thesis, Florida State University, Tallahassee, Florida, 2006.

[5] Maksimovic, Zane, and Erickson, "Impact of digital control in power electronics," in *2004 Proceedings of the 16th International Symposium on Power Semiconductor Devices and ICs*, pp. 13–22, 2004.

[6] T. Nabeshima and K. Harada, "Large-signal transient responses of a switching regulator," *IEEE Transactions on Aerospace and Electronic Systems*, vol. AES-18, no. 5, pp. 545–551, 1982.

[7] J. Mahdavi, A. Emaadi, M. D. Bellar, and M. Ehsani, "Analysis of power electronic converters using the generalized state-space averaging approach," *IEEE Transactions on Circuits and Systems I: Fundamental Theory and Applications*, vol. 44, no. 8, pp. 767–770, 1997.

[8] K. Natarajan and M. Yektaii, "Modeling of dc–dc buck converters for large-signal frequency response and limit cycles," *IEEE Transactions on Circuits and Systems II: Express Briefs*, vol. 53, no. 8, pp. 712–716, 2006.

[9] R. D. Middlebrook, "Small-signal modeling of pulse-width modulated switched-mode power converters," *Proceedings of the IEEE*, vol. 76, no. 4, pp. 343–354, 1988.

[10] D. G. Luenberger, “Observing the state of a linear system,” *IEEE Transactions on Military Electronics*, vol. 8, no. 2, pp. 74–80, 1964.

[11] D. Luenberger, “An introduction to observers,” *IEEE Transactions on Automatic Control*, vol. 16, no. 6, pp. 596–602, 1971.

[12] L. A. McGee and S. F. Schmidt, “Discovery of the Kalman filter as a practical tool for aerospace and industry,” *NASA Technical Memorandum 86847*, 11 1985.

[13] Q. Li, R. Li, K. Ji, and W. Dai, “Kalman filter and its application,” in *2015 8th International Conference on Intelligent Networks and Intelligent Systems (ICINIS)*, pp. 74–77, 2015.

[14] D. Simon, *Optimal State Estimation: Kalman, H Infinity, and Nonlinear Approaches*. USA: Wiley-Interscience, 2006.

[15] R. Kopp and R. Orford, “Linear regression applied to system identification for adaptive control systems,” *AIAA Journal*, vol. 1, pp. 2300–2306, 1963.

[16] R. Dhaouadi, N. Mohan, and L. Norum, “Design and implementation of an extended kalman filter for the state estimation of a permanent magnet synchronous motor,” *IEEE Transactions on Power Electronics*, vol. 6, no. 3, pp. 491–497, 1991.

[17] W. Zhang, S. Wong, C. K. Tse, and Q. Chen, “Design for efficiency optimization and voltage controllability of series–series compensated inductive power transfer systems,” *IEEE Transactions on Power Electronics*, vol. 29, no. 1, pp. 191–200, 2014.

[18] G. Benelli and A. Pozzebon, *RFID Under Water: Technical Issues and Applications, Radio Frequency Identification from System to Applications*. IntechOpen, first ed., 2013.

[19] M. Y. Candan and M. M. Ankarali, “Extended kalman filter based state and parameter estimation method for a buck converter operating in a wide load range,” in *2020 IEEE Energy Conversion Congress and Exposition (ECCE)*, pp. 3238–3244, 2020.

[20] J. A. Sabate, V. Vlatkovic, R. B. Ridley, F. C. Lee, and B. H. Cho, “Design considerations for high-voltage high-power full-bridge zero-voltage-switched pwm converter,” in *Fifth Annual Proceedings on Applied Power Electronics Conference and Exposition*, pp. 275–284, 1990.

[21] R. Redl, N. O. Sokal, and L. Balogh, “A novel soft-switching full-bridge dc/dc converter: analysis, design considerations, and experimental results at 1.5 kw, 100 khz,” *IEEE Transactions on Power Electronics*, vol. 6, no. 3, pp. 408–418, 1991.

[22] D. B. Dalal, “A 500 khz multi-output converter with zero voltage switching,” in *Fifth Annual Proceedings on Applied Power Electronics Conference and Exposition*, pp. 265–274, 1990.

[23] M. Ilic and D. Maksimovic, “Phase-shifted full bridge dc-dc converter with energy recovery clamp and reduced circulating current,” in *APEC 07 - Twenty-Second Annual IEEE Applied Power Electronics Conference and Exposition*, pp. 969–975, 2007.

[24] D. S. Gautam, F. Musavi, W. Eberle, and W. G. Dunford, “A zero-voltage switching full-bridge dc–dc converter with capacitive output filter for plug-in hybrid electric vehicle battery charging,” *IEEE Transactions on Power Electronics*, vol. 28, no. 12, pp. 5728–5735, 2013.

[25] W. Lee, C. Kim, G. Moon, and S. Han, “A new phase-shifted full-bridge converter with voltage-doubler-type rectifier for high-efficiency pdp sustaining power module,” *IEEE Transactions on Industrial Electronics*, vol. 55, no. 6, pp. 2450–2458, 2008.

[26] M. Pahlevaninezhad, P. Das, J. Drobnik, P. K. Jain, and A. Bakhshai, “A novel zvzcs full-bridge dc/dc converter used for electric vehicles,” *IEEE Transactions on Power Electronics*, vol. 27, no. 6, pp. 2752–2769, 2012.

[27] W. Cha, J. Kwon, and B. Kwon, “Highly efficient asymmetrical pwm full-bridge converter for renewable energy sources,” *IEEE Transactions on Industrial Electronics*, vol. 63, no. 5, pp. 2945–2953, 2016.

[28] K. Domoto, Y. Ishizuka, S. Abe, and T. Ninomiya, "Output-inductor-less full-bridge converter with sic-mosfets for low noise and zvs operation," in *2016 IEEE Applied Power Electronics Conference and Exposition (APEC)*, pp. 2422–2429, 2016.

[29] Y. Xie, R. Ghaemi, J. Sun, and J. S. Freudenberg, "Model predictive control for a full bridge dc/dc converter," *IEEE Transactions on Control Systems Technology*, vol. 20, no. 1, pp. 164–172, 2012.

[30] O. Ibrahim, N. Z. Yahaya, N. Saad, and K. Y. Ahmed, "Development of observer state output feedback for phase-shifted full bridge dc–dc converter control," *IEEE Access*, vol. 5, pp. 18143–18154, 2017.

[31] J. Lu, S. Golestan, M. Savaghebi, J. C. Vasquez, J. M. Guerrero, and A. Marzabal, "An enhanced state observer for dc-link voltage control of three-phase ac/dc converters," *IEEE Transactions on Power Electronics*, vol. 33, no. 2, pp. 936–942, 2018.

[32] J. Lu, M. Savaghebi, Y. Guan, J. C. Vasquez, A. M. Y. M. Ghias, and J. M. Guerrero, "A reduced-order enhanced state observer control of dc-dc buck converter," *IEEE Access*, vol. 6, pp. 56184–56191, 2018.

[33] S. K. Pandey, S. L. Patil, U. M. Chaskar, and S. B. Phadke, "State and disturbance observer-based integral sliding mode controlled boost dc–dc converters," *IEEE Transactions on Circuits and Systems II: Express Briefs*, vol. 66, no. 9, pp. 1567–1571, 2019.

[34] A. G. Beccuti, S. Mariethoz, S. Cliquennois, S. Wang, and M. Morari, "Explicit model predictive control of dc–dc switched-mode power supplies with extended kalman filtering," *IEEE Transactions on Industrial Electronics*, vol. 56, no. 6, pp. 1864–1874, 2009.

[35] *Murata Power Solutions, DC-DC Converters, Application Notes*, (accessed May 2020). `https://www.murata.com/-/media/webrenewal/products/power/appnote/dcan-68.pdf`.

[36] S. F. Lim and A. M. Khambadkone, "A simple digital dcm control scheme for

boost pfc operating in both ccm and dcm," *IEEE Transactions on Industry Applications*, vol. 47, no. 4, pp. 1802–1812, 2011.

[37] C. H. van der Broeck, R. W. De Doncker, S. A. Richter, and J. v. Bloh, "Unified control of a buck converter for wide-load-range applications," *IEEE Transactions on Industry Applications*, vol. 51, no. 5, pp. 4061–4071, 2015.

[38] V. Vorperian, "Simplified analysis of pwm converters using model of pwm switch. continuous conduction mode," *IEEE Transactions on Aerospace and Electronic Systems*, vol. 26, no. 3, pp. 490–496, 1990.

[39] V. Vorperian, "Simplified analysis of pwm converters using model of pwm switch. ii. discontinuous conduction mode," *IEEE Transactions on Aerospace and Electronic Systems*, vol. 26, no. 3, pp. 497–505, 1990.

[40] D. Czarkowski and M. K. Kazimierczuk, "Energy-conservation approach to modeling pwm dc-dc converters," *IEEE Transactions on Aerospace and Electronic Systems*, vol. 29, no. 3, pp. 1059–1063, 1993.

[41] N. Femia and V. Tucci, "On the modeling of pwm converters for large signal analysis in discontinuous conduction mode," *IEEE Transactions on Power Electronics*, vol. 9, no. 5, pp. 487–496, 1994.

[42] R. D. Middlebrook and S. Cuk, "A general unified approach to modelling switching-converter power stages," in *1976 IEEE Power Electronics Specialists Conference*, pp. 18–34, 1976.

[43] S. Buso, "Design of a robust voltage controller for a buck-boost converter using /spl mu/-synthesis," *IEEE Transactions on Control Systems Technology*, vol. 7, no. 2, pp. 222–229, 1999.

[44] C. H. Rivetta, A. Emadi, G. A. Williamson, R. Jayabalan, and B. Fahimi, "Analysis and control of a buck dc-dc converter operating with constant power load in sea and undersea vehicles," *IEEE Transactions on Industry Applications*, vol. 42, no. 2, pp. 559–572, 2006.

[45] C. M. Liaw and S. J. Chiang, "Robust control of multimodule current-mode controlled converters," *IEEE Transactions on Power Electronics*, vol. 8, no. 4, pp. 455–465, 1993.

[46] Y. Zhao, W. Qiao, and D. Ha, "A sliding-mode duty-ratio controller for dc/dc buck converters with constant power loads," *IEEE Transactions on Industry Applications*, vol. 50, no. 2, pp. 1448–1458, 2014.

[47] S. Saggini, M. Ghioni, and A. Geraci, "An innovative digital control architecture for low-voltage, high-current dc-dc converters with tight voltage regulation," *IEEE Transactions on Power Electronics*, vol. 19, no. 1, pp. 210–218, 2004.

[48] A. H. Jazwinski, *Stochastic Processes and Filtering Theory*. San Diego: CA: Academic, 1970.

[49] H. W. Sorenson, *Kalman Filtering: Theory and Application*. Piscataway: NJ: IEEE, 1985.

[50] S. J. Julier and J. K. Uhlmann, "Unscented filtering and nonlinear estimation," *Proceedings of the IEEE*, vol. 92, no. 3, pp. 401–422, 2004.

[51] L. Frenkel and M. Feder, "Recursive expectation-maximization (em) algorithms for time-varying parameters with applications to multiple target tracking," *IEEE Transactions on Signal Processing*, vol. 47, no. 2, pp. 306–320, 1999.

[52] G. Feng, C. Lai, and N. C. Kar, "Expectation-maximization particle-filter- and kalman-filter-based permanent magnet temperature estimation for pmsm condition monitoring using high-frequency signal injection," *IEEE Transactions on Industrial Informatics*, vol. 13, no. 3, pp. 1261–1270, 2017.

[53] E. Özkan, F. Lindsten, C. Fritsche, and F. Gustafsson, "Recursive maximum likelihood identification of jump markov nonlinear systems," *IEEE Transactions on Signal Processing*, vol. 63, no. 3, pp. 754–765, 2015.

APPENDIX A

MATLAB SIMULINK MODEL FOR "LINEARIZED KALMAN OBSERVER BASED CONTROL FOR A FULL-BRIDGE DC/DC CONVERTER WITHOUT OUTPUT VOLTAGE MEASUREMENT" STUDY

We simulate the proposed Linearized Kalman Observer based control for a Full-Bridge DC/DC converter in MATLAB Simulink environment. For the circuit model components we use *Simscape/Power Systems/Specialized Technology* library. Model configuration solver parameters are given in Figure A.1.

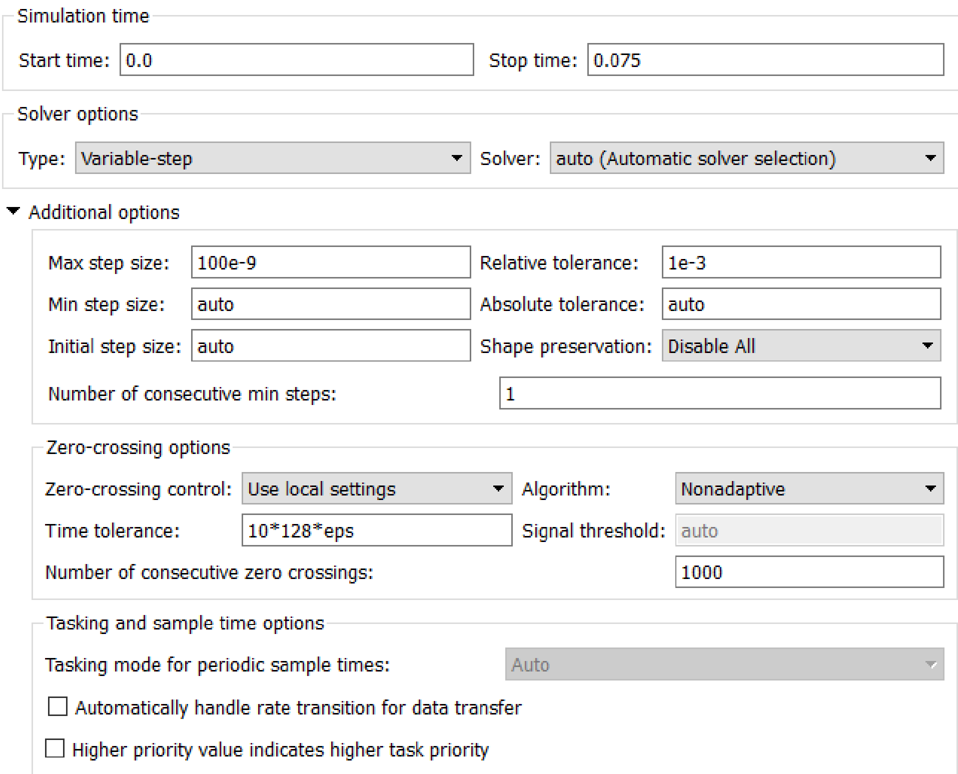

Figure A.1: Model configuration solver parameters in MATLAB Simulink

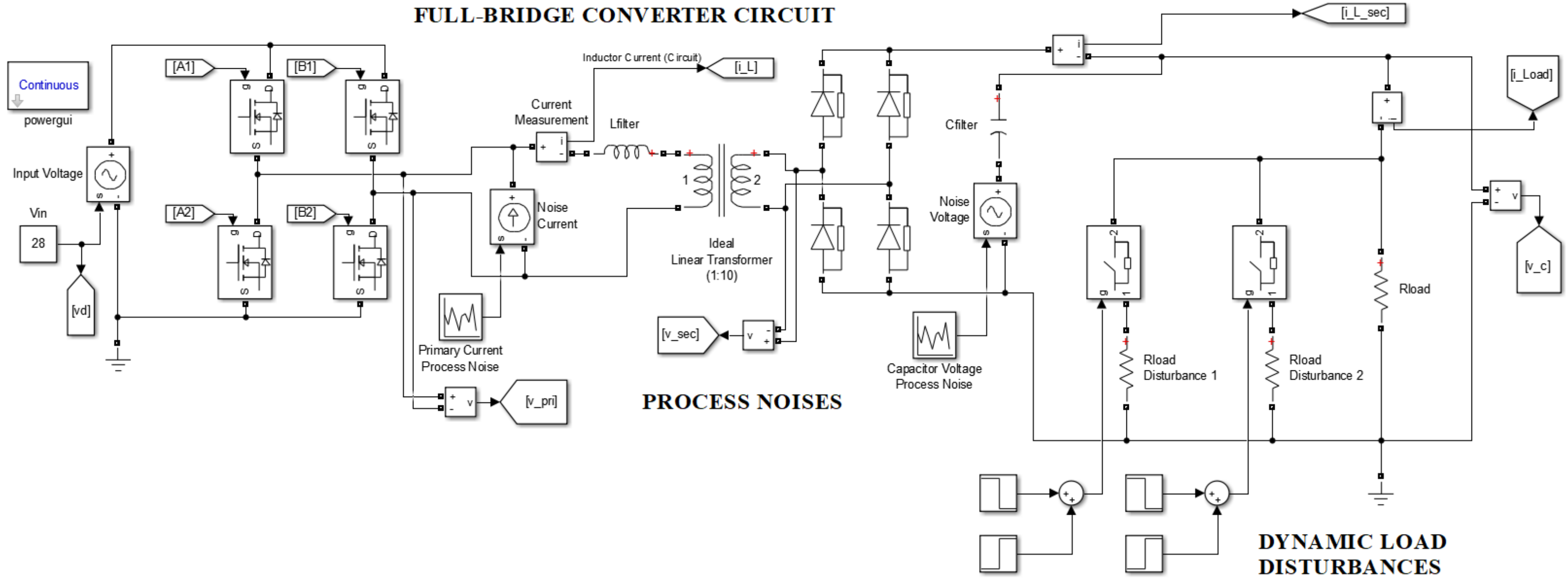

Figure A.2: Output Inductor-less Phase-Shifted Full-Bridge converter circuit model in MATLAB Simulink

Output Inductor-less Phase-Shifted Full-Bridge converter circuit model is shown in Figure A.2 where we add the inductor current process noise and capacitor voltage process noise as parallel current source and series voltage source, respectively. We generate the noises using *Random Source* block. As an example, the primary current process noise source block is given in Figure A.3.

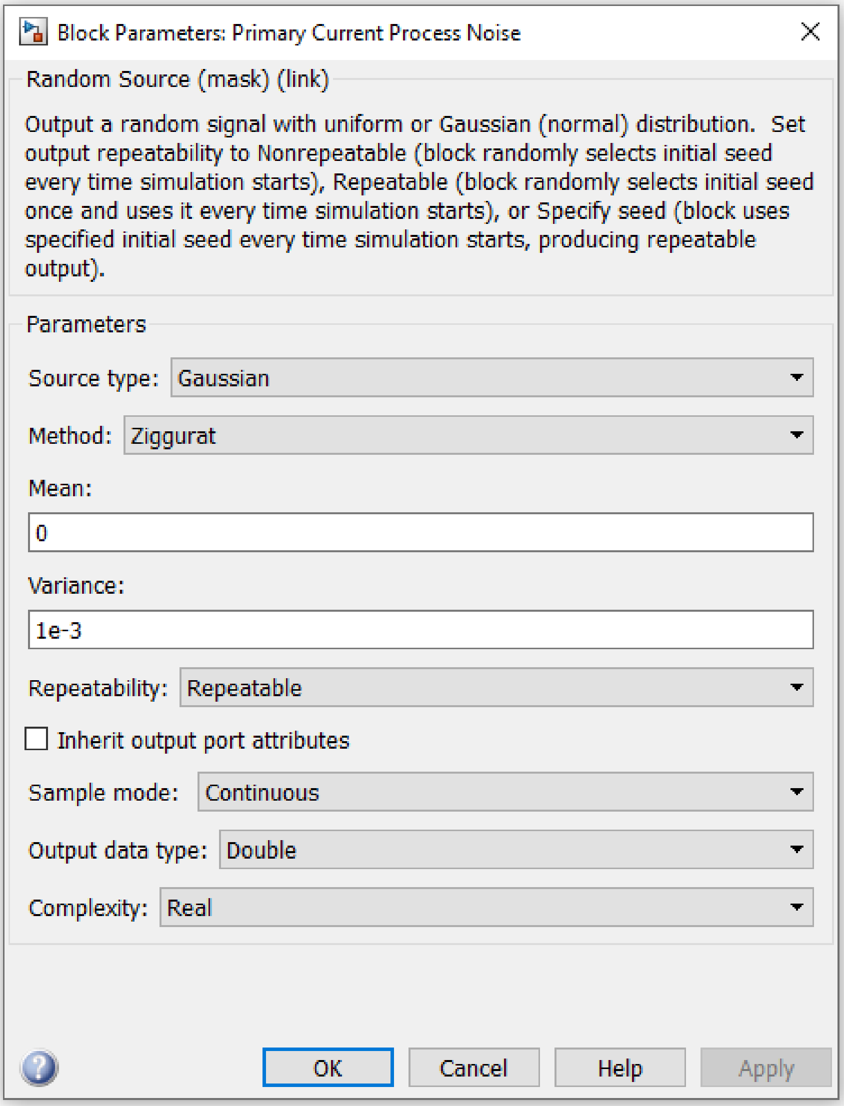

Figure A.3: Primary current process noise source block parameters

The voltage controller and gate driver signal generator is depicted in Figure A.4. We use a simple PID controller block with output limit and anti-windup. PID block parameters are given in Table A.1.

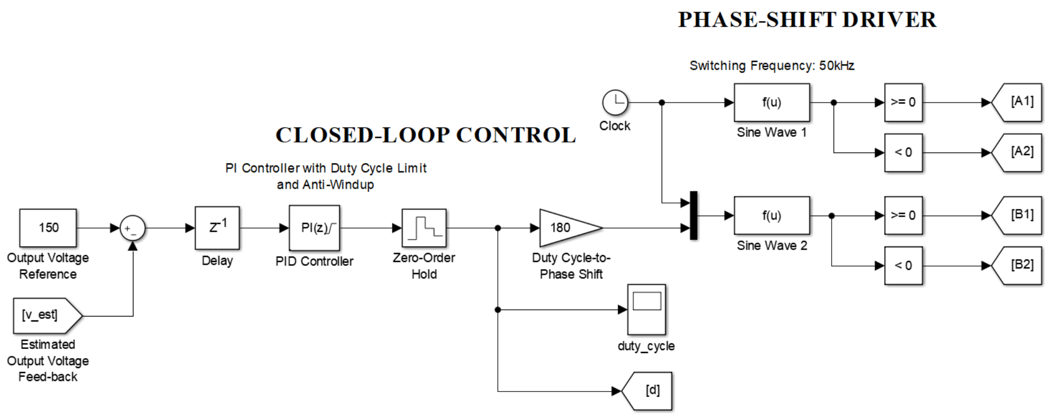

Figure A.4: Proportional-Integral-Derivative Controller structure and Phase-Shifted Full-Bridge gate driver signal generator blocks

Table A.1: Proportional-Integral Controller Block Parameters for the Full-Bridge Converter Study

Controller	PI
Time domain	Discrete-time
Source	Internal
Proportional (P)	6.87e-05
Integral (I)	6.87
Upper saturation limit	1
Lower saturation limit	0
Anti-windup method	Clamping
Integrator method	Forward Euler
Sample time	2e-05

We convert the duty cycle to phase-shift and generate gate signals using function blocks with following expressions:

```
Sine Wave 1 Expression:
sin(2*pi*50000*u(1))

Sine Wave 2 Expression:
sin(2*pi*50000*u(1) - (u(2)*pi/180))
```

In this study, we measure the AC primary inductor current, we rectify, filter and reflect it to the secondary side. We add the measurement noise in the same way as we discussed for the process noise. The following figure shows the related model.

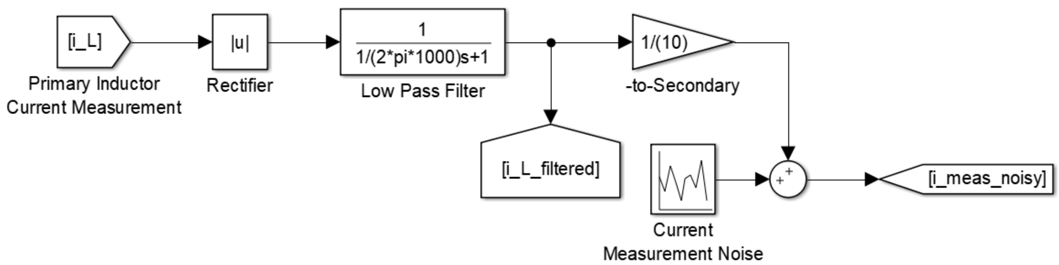

Figure A.5: Manipulation of the primary current (rectification, filtering and reflection) and measurement noise addition

Linearized Kalman Observer block takes noisy current measurement, duty cycle and secondary side reflected input voltage (modulation voltage). It outputs the observation of current and voltage states and estimation of the load resistance.

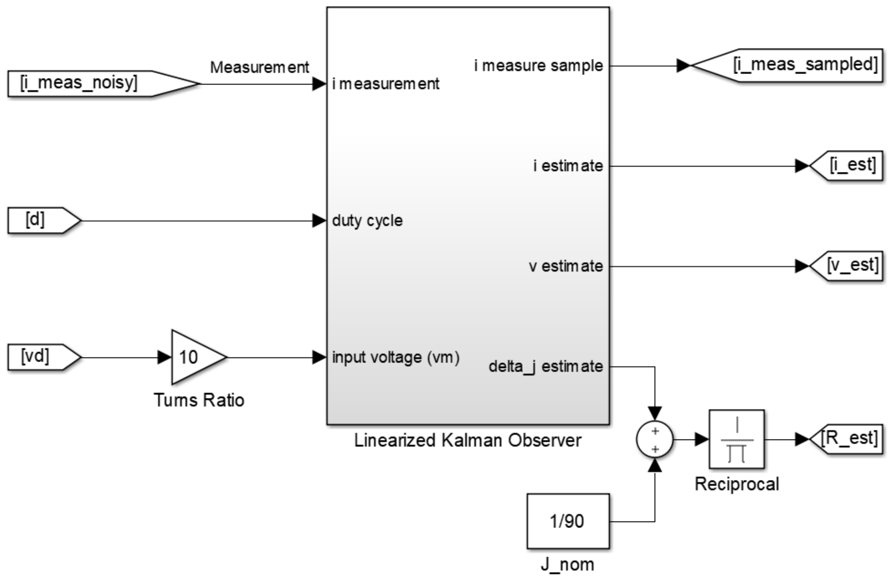

Figure A.6: Linearized Kalman Observer block

Inside of the Observer block there is a *Zero Order Hold* block for sampling the measurement, and *Delay* block for each output variable to satisfy the evolution of the algorithm as shown in Figure A.7. In the following section the code executed for Linearized Kalman Filter algorithm is presented.

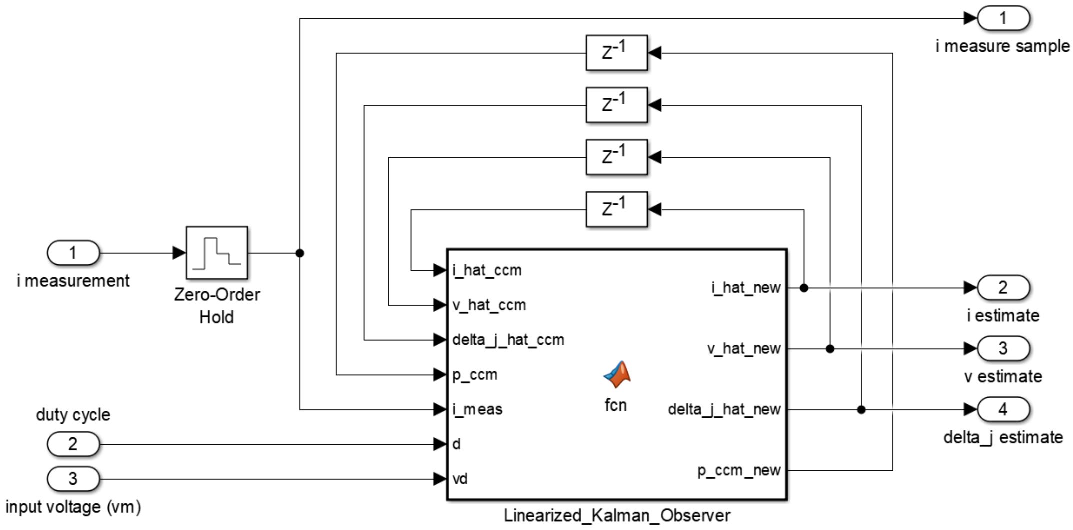

Figure A.7: Inside of the Linearized Kalman Observer block

A.1 Linearized Kalman Filter MATLAB Function Code

```
function [i_hat_new, v_hat_new, delta_j_hat_new, p_dcm_new]...
= fcn(i_hat_dcm, v_hat_dcm, delta_j_hat_dcm, p_dcm, i_meas, d, vd)

% x1=if .... x2=vO .... x3=g=1/r
C = [1 0 0];

% Covariances
Q = [1e-4 0 0; 0 1e-3 0; 0 0 1e-9];
R = [5e-3];

% Circuit parameters
Vcnom = 150; %output voltage reference
Rload = 90; %output resistor
Jload = 1/Rload; %conductance
Lfilter = 1.75e-6 * 10^2; %filter inductor
Cfilter = 10e-6; %filter capacitor
Ts = 1/(100e3); %switching period of the secondary
Z0 = sqrt(Lfilter/Cfilter); %resonant impedance
w0 = 1/sqrt(Lfilter*Cfilter); %resonant frequency
dnom = 0.495; %nominal duty cycle

% State vector and measurements
xhatdcm = [i_hat_dcm; v_hat_dcm; delta_j_hat_dcm];
y = [i_meas];

% Prediction step

xhatdcm_new = [xhatdcm(2)*(Jload+xhatdcm(3));...

               ((d^2*(w0*Ts)^2*(vd-xhatdcm(2))^2)/...
               (xhatdcm(2)-(Z0*w0*Ts*d*xhatdcm(2))*(Jload+xhatdcm(3))))-...
               (Z0*w0*Ts*xhatdcm(2)*(Jload+xhatdcm(3)))+xhatdcm(2);...

               xhatdcm(3)];
```

```
Fdcm = [0      Jload      Vcnom;

        0

         (1-(Z0*w0*Ts)*Jload)+((dnom^2*(w0*Ts)^2)/...
         (1-(Z0*w0*Ts*dnom)*Jload))*((Vcnom^2 - vd^2)/(Vcnom^2))

         (dnom^2*(w0*Ts)^2*(vd-Vcnom)^2*(Z0*w0*Ts*dnom*Vcnom))/...
         ((Vcnom-Z0*w0*Ts*dnom*Vcnom*Jload)^2)-Z0*w0*Ts*Vcnom;

        0      0          1];

Ldcm = [1 0 0; 0 1 0; 0 0 1];
Pdcm = Fdcm * p_dcm * Fdcm' + Ldcm * Q * Ldcm';

% Update step
Sdcm = C * Pdcm * C' + R;
Kdcm = Pdcm * C' * pinv(Sdcm); %kalman gain
xhatdcm_new = xhatdcm_new + Kdcm * ( y - C * xhatdcm_new );
Pdcm = (eye(3) - Kdcm * C) * Pdcm;


% Limits
if (xhatdcm_new(1) <= 0)
    xhatdcm_new(1) = 0;
end

if (xhatdcm_new(2) <= 1)
    xhatdcm_new(2) = 1;
end

i_hat_new = xhatdcm_new(1);
v_hat_new = xhatdcm_new(2);
delta_j_hat_new = xhatdcm_new(3);
p_dcm_new = Pdcm;
```

APPENDIX B

MATLAB SIMULINK MODEL FOR "EXTENDED KALMAN FILTER BASED STATE AND PARAMETER ESTIMATION METHOD FOR A BUCK CONVERTER OPERATING IN A WIDE LOAD RANGE" STUDY

We simulate the proposed Extended Kalman Filter based state and parameter estimator for a DC/DC Buck converter in MATLAB Simulink environment. For the circuit model components we use *Simscape/Power Systems/Specialized Technology* library. Model configuration solver parameters are the same as given in Appendix A.

Buck converter circuit model is shown in Figure B.2 where we add the inductor current process noise and capacitor voltage process noise as parallel current source and series voltage source, respectively. We add the measurement noises directly as it can be seen in Figure B.1. Also, we generate the noises using *Random Source* block as detailed in Appendix A.

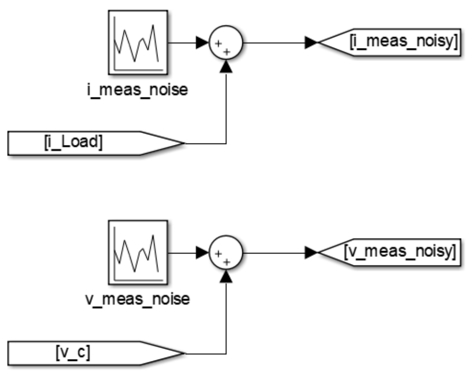

Figure B.1: Measurement noise addition

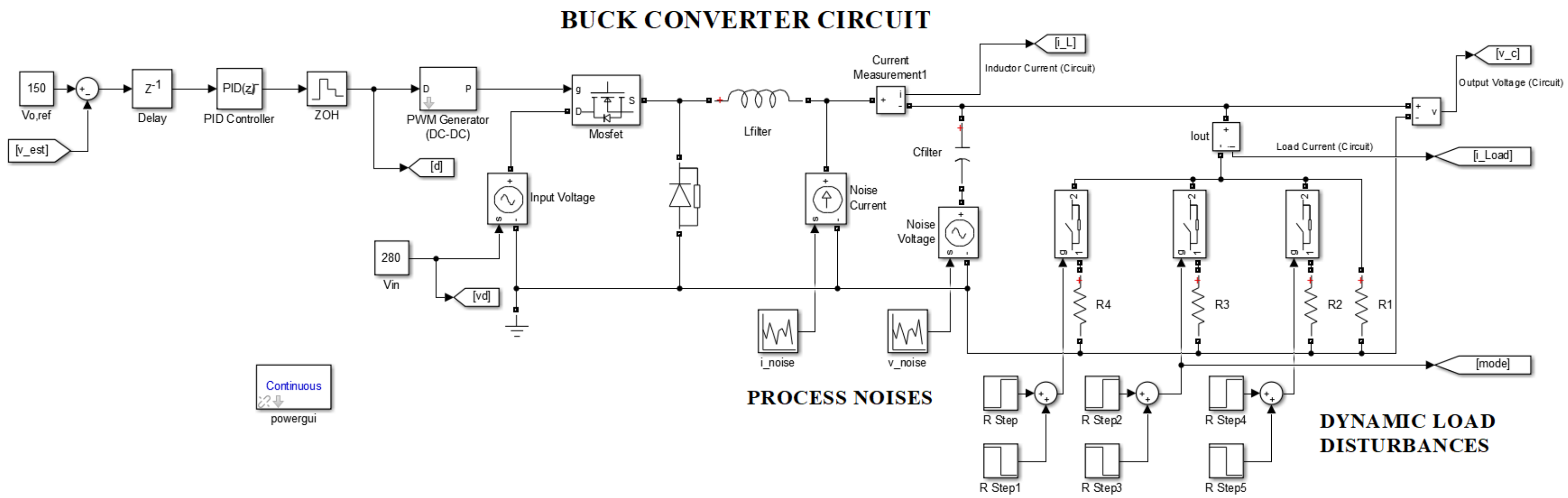

Figure B.2: Buck converter circuit model in MATLAB Simulink

We use a simple PID controller block with output limit and anti-windup. PID block parameters are given in Table B.1.

Table B.1: Proportional-Integral Controller Block Parameters for the Buck Converter Study

Controller	PI
Time domain	Discrete-time
Source	Internal
Proportional (P)	8.35e-05
Integral (I)	16.7
Upper saturation limit	1
Lower saturation limit	0
Anti-windup method	Clamping
Integrator method	Forward Euler
Sample time	10e-6

Kalman Filter estimator block takes noisy load current and capacitor voltage measurement as well as duty cycle and input voltage. It outputs the observation of current and voltage states and estimation of the load resistance and operation mode.

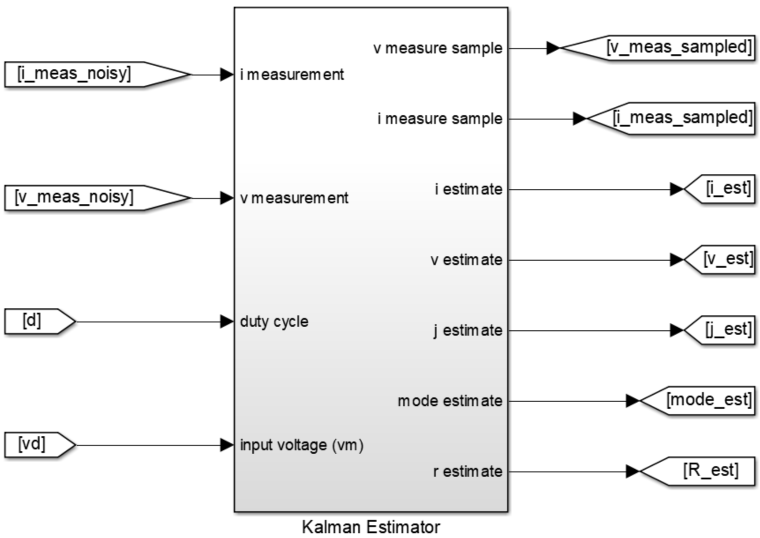

Figure B.3: Extended Kalman Filter estimator block

Inside of the estimator block there are *Zero Order Hold* blocks for sampling the measurements and *Delay* blocks for each output variable to satisfy the evolution of the algorithms as shown in Figure B.4. In the following sections the codes executed for Extended Kalman Filter algorithms for both CCM and DCM are presented.

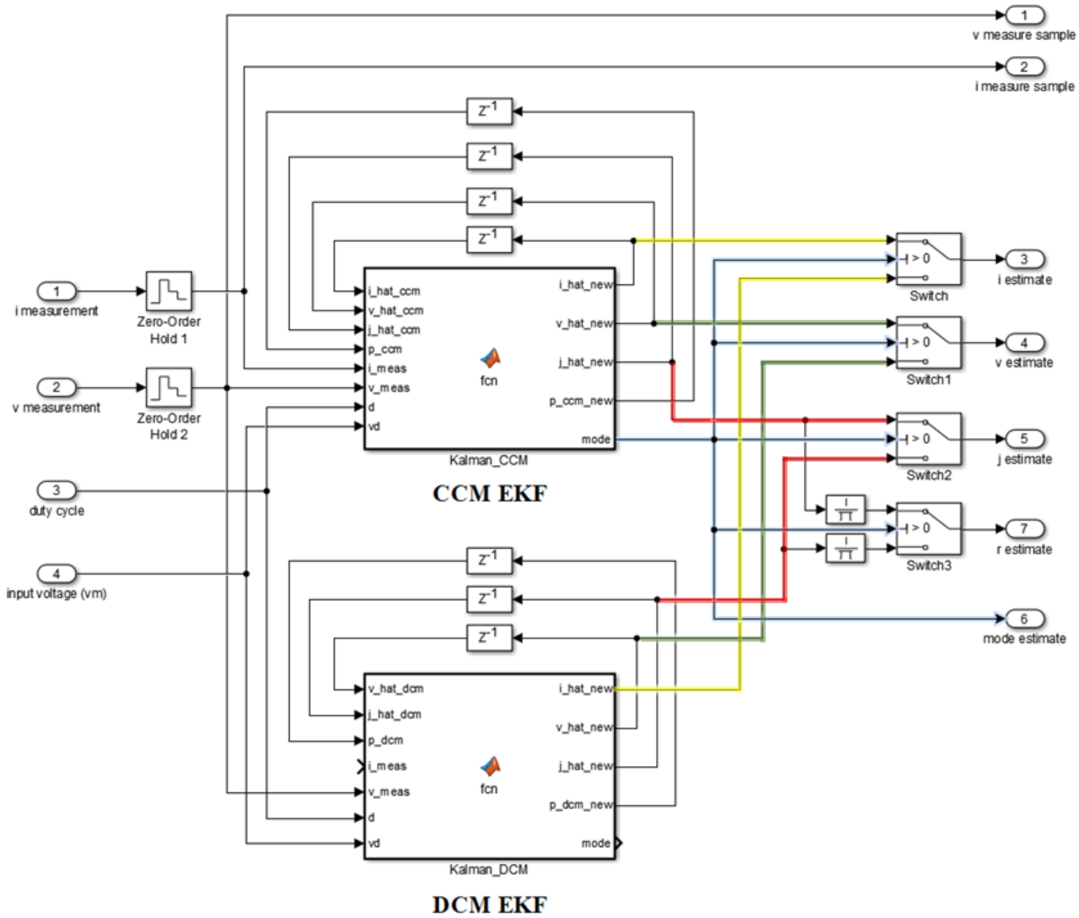

Figure B.4: Inside of the Extended Kalman Filter estimator block

B.1 CCM Buck Converter Extended Kalman Filter MATLAB Function Code

```
function [i_hat_new, v_hat_new, j_hat_new, p_ccm_new, mode]...
= fcn(i_hat_ccm, v_hat_ccm, j_hat_ccm, p_ccm, i_meas, v_meas, d, vd)
% x1=iLoad .... x2=vC .... x3=J=1/R
C = [1 0 0; 0 1 0];

% Covariances
Qccm = [1e-4 0 0; 0 1e-3 0; 0 0 1e-10];
R = [5e-3 0; 0 1];

% Conductance limit
if (j_hat_ccm <= 0)
    j_hat_ccm = 1/2500;
end

% Circuit parameters
Lfilter = 350e-6; %filter inductor
Cfilter = 1e-6; %filter capacitor
Ts = 1/100e3; %switching period
Z0 = sqrt(Lfilter/Cfilter); %resonant impedance
w0 = 1/sqrt(Lfilter*Cfilter); %resonant frequency

% State vector and measurements
xhatccm = [i_hat_ccm; v_hat_ccm; j_hat_ccm];
y = [i_meas; v_meas];

% Prediction step
u = d*vd; %input

xhatccm_new = [cos(w0*Ts)*xhatccm(1)+(-sin(w0*Ts)/Z0)*xhatccm(2)+...
(xhatccm(2)*xhatccm(3))*(1-cos(w0*Ts))+(sin(w0*Ts)/Z0)*u;...

Z0*sin(w0*Ts)*xhatccm(1)+(cos(w0*Ts))*xhatccm(2)+...
(xhatccm(2)*xhatccm(3))*(-(Z0*sin(w0*Ts)))+(1-cos(w0*Ts))*u;...

xhatccm(3)];
```

```
% F = del(F)/del(x) @ xhat
Fccm = [cos(w0*Ts)     ((-sin(w0*Ts))/Z0)+(1-cos(w0*Ts))*xhatccm(3)
        (1-cos(w0*Ts))*xhatccm(2);

        Z0*sin(w0*Ts)  cos(w0*Ts)-Z0*sin(w0*Ts)*xhatccm(3)
        (-Z0*sin(w0*Ts))*xhatccm(2);

        0 0 1];
Lccm = [1 0 0; 0 1 0; 0 0 1];
Pccm = Fccm * p_ccm * Fccm' + Lccm * Qccm * Lccm';

% Update step
Sccm = C * Pccm * C' + R;
Kccm = Pccm * C' * pinv(Sccm); %kalman gain
xhatccm_new = xhatccm_new + Kccm * ( y - C * xhatccm_new );
Pccm = (eye(3) - Kccm * C) * Pccm;

% Limits
if (xhatccm_new(1) <= 0)
    xhatccm_new(1) = 0;
end

if (xhatccm_new(2) <= 1)
    xhatccm_new(2) = 1;
end

if (xhatccm_new(3) <= 1/2500)
    xhatccm_new(3) = 1/2500;
end

i_hat_new = xhatccm_new(1);
v_hat_new = xhatccm_new(2);
j_hat_new = xhatccm_new(3);
p_ccm_new = Pccm;
```

```
% Mode detection
if (abs(v_hat_new - v_meas) < v_meas * 0.1)
    mode = 1; %CCM
else
    mode = 0; %DCM
end
```

B.2 DCM Buck Converter Extended Kalman Filter MATLAB Function Code

```
function [i_hat_new, v_hat_new, j_hat_new, p_dcm_new, mode]...
= fcn(v_hat_dcm, j_hat_dcm, p_dcm, i_meas, v_meas, d, vd)
% x1=iL .... x2=vC .... x3=J=1/R
C = [1 0];

% Covariances
Qdcm = [1e-3 0; 0 1e-10];
R = 1;

% Circuit parameters
Lfilter = 350e-6; %filter inductor
Cfilter = 1e-6; %filter capacitor
Ts = 1/100e3; %switching period
Z0 = sqrt(Lfilter/Cfilter); %resonant impedance
w0 = 1/sqrt(Lfilter*Cfilter); %resonant frequency

% Voltage and conductance limit
if (v_hat_dcm <= 1)
    v_hat_dcm = 1;
end

if (j_hat_dcm <= 1/2500)
    j_hat_dcm = 1/2500;
end

% State vector and measurements
xhat = [v_hat_dcm; j_hat_dcm];
y = [v_meas];

% Prediction step
xhat_new = [((d^2*(w0*Ts)^2*(vd-xhat(1))^2)/(xhat(1)-...
            (Z0*w0*Ts*d*xhat(1))*xhat(2)))-...
            (Z0*w0*Ts*xhat(1)*xhat(2))+xhat(1);

            xhat(2)];
```

```
% F = del(f)/del(x) @ xhat
F = [(1-(Z0*w0*Ts)*xhat(2))+((d^2*(w0*Ts)^2)/...
    (1-(Z0*w0*Ts*d)*xhat(2)))*((xhat(1)^2 - vd^2)/(xhat(1)^2)) ...

    (d^2*(w0*Ts)^2*(vd-xhat(1))^2*(Z0*w0*Ts*d*xhat(1)))/...
    ((xhat(1)-Z0*w0*Ts*d*xhat(1)*xhat(2))^2)-Z0*w0*Ts*xhat(1);

    0 1];
L = [1 0; 0 1];
P = F * p_dcm * F' + L * Qdcm * L';

% Update step
S = C * P * C' + R;
K = P * C' * pinv(S); %kalman gain
xhat_new = xhat_new + K * ( y - C * xhat_new );
P = (eye(2) - K * C) * P;

% Limits
if (xhat_new(1) <= 1)
    xhat_new(1) = 1;
end

if (xhat_new(2) <= 1/2500)
    xhat_new(2) = 1/2500;
end

i_hat_new = i_meas;
v_hat_new = xhat_new(1);
j_hat_new = xhat_new(2);
p_dcm_new = P;
```